

Partial ionisation cross sections for the binary-encounter Bethe model.

Anthony Jeseněk†, Alejandro Luque‡, Nikolai Lehtinen‡

†Instituto de Astrofísica de Andalucía, Granada, 18008, España

‡Birkeland Center for Space Science, University of Bergen

E-mail: anthony.schmalzried@mailfence.com

E-mail: aluque@iaa.es

E-mail: nikolai.lehtinen@uib.no

July 2025

Abstract. The original binary-encounter Bethe model of Kim and Rudd [48] has proven to be an accurate analytical representation of total impact ionisation cross sections of electrons colliding with atoms and molecules. It is based on a decomposition into partial ionisation cross sections from electrons in bound orbitals. Despite the model's accuracy for *total* ionisation, its individual *partial* cross sections for ionisation rely on thresholds calculated theoretically which systematically overestimate the experimental orbital binding energies. Here, we examine the BEB model's performance when based on experimental ionisation thresholds. The resulting partial cross sections of the various final (excited) ionic states produced could help to prefigure subsequent optical radiations and non-radiative transitions in models of plasma physics.

1. Introduction

Electron impact ionisation on atmospheric molecules is an important process in plasmas where the average kinetic energy of the electrons is near or above the ionisation threshold of the medium species. Analytical representations of cross sections are an economical and efficient way of modelling impact ionisation. There exist many semi-empirical or empirical formulae that accurately represent total ionisation cross sections [17, 36, 61], reviewed in Younger and Märk [93]. Among these, the binary-encounter Bether (BEB) model gives remarkable results while requiring as external input only values of the electron kinetic U and binding B energies in occupied atomic or molecular orbitals. With theoretically calculated values of U and B , except for the *lowest* ionisation threshold determined experimentally, the BEB was successfully applied for modelling total ionisation cross sections from atoms [47, 48], diatomic molecules [34, 36] and other polyatomic atmospheric molecules [46].

The *total* ionisation cross section σ_{ion} is the sum of all *partial* cross sections from ionisation processes in which the ion is left in the ground or an excited state. When

interested in tracking these excited ionic species or accurately modelling electron energy losses in ionisation, it is important to distinguish different partial ionisation channels. In principle, the BEB model already gives a decomposition of these partial processes according to the theoretical orbital structure of the target atom or molecule. In practice, however, these partial processes may *not* be thus modelled, as they do not reflect the experimental *threshold* nor the actual ionisation process determined by the transition from the ground neutral state to the final (excited) ionic state.

In this paper, we discuss how can the BEB model be adapted to model partial processes of ionisation useful in Monte Carlo [12, 16, 53, 54, 73] or kinetic [29, 70, 81] modelling of electron swarms in gaseous media. We begin in the next section (2) by reminding the reader about the BEB model and restating its fundamental assumptions. For each assumption, we also present its drawbacks. Then, in section 3, we introduce another perspective of the BEB, not based on orbital structure but on ionisation channels and we argue why we think it is a more appropriate application. This new perspective, we illustrate in section (4), where we apply the BEB model to the impact ionisation of electrons on simple atomic and molecular gas targets relevant for atmospheric studies. At the end, we present a conclusion (5) and an outlook for the BEB model for partial ionisation.

2. The orbital binary-encounter Bethe model

The binary-encounter Bethe model is based on a Born approximation combining long-range dipole interaction and terms from the Mott cross section between two electrons for close-range binary encounters. As we are interested here to represent partial cross sections at energies of at most a few hundred eVs, we present the non-relativistic formula for the sake of simplicity. For an incident electron at a kinetic energy ε , the partial ionisation cross section at a threshold I_j from an orbital j hosting N_j electrons is given by [49, eq.(11)]:

$$\sigma_j(\varepsilon) = \frac{4\pi a_0^2 N_j \text{Ryd}^2}{\varepsilon + K_j} \frac{1}{I_j} \left[\frac{1}{2} \ln(\varepsilon/I_j) \left(1 - \left(\frac{I_j}{\varepsilon} \right)^2 \right) + 1 - \frac{I_j}{\varepsilon} - \frac{\ln(\varepsilon/I_j)}{1 + \varepsilon/I_j} \right], \quad (1)$$

with the atomic Bohr radius $a_0 \approx 5.291 \times 10^{-11}$ m and Rydberg energy $\text{Ryd} \approx 13.602$ eV. In addition to the assumptions underlying the Bethe approximation, the BEB formula (1) assumes that:

- a) The parameter K_j represents the gain in kinetic energy of the incident electron at the place where ionisation takes place;
- b) The dipole oscillator strength density, depending on the secondary electron kinetic energy w , follows a simple analytical form (7) $\propto 1/(w + I_j)^2$;
- c) The Bethe sum of the dipole oscillator strength is fully due to ionisation, i.e. the contribution of all discrete optically allowed excitations is accounted in the magnitude of the BEB model [48, $Q = 1$ assumption on p.3959 at the end of §IV.];

- d) The values of K_j and I_j can be obtained from the kinetic U_j and binding B_j energies of electrons in the orbitals constituting the neutral target molecule based on a Hartree-Fock description.

2.1. The scaling parameter K_j

The value K_j is an empirical scaling which accounts for the acceleration of the incident electron in the attractive potential of the target. As it relies on the Born approximation, without this scaling, the BEB model would significantly overestimate the ionisation cross section. Therefore, the K_j scaling buttresses the success of the BEB model by effectively lowering the cross section at energies near threshold (where the Born approximation fails).

At the same time, K_j is the Achilles' heel of the BEB because there is no universal formula for estimating K_j that would befit all sorts of impact ionisation cross sections. Instead, several semi-empirical variants have been proposed in order to extend the applicability of the BEB to a variety of targets: light/heavy atoms [28], valence/core orbitals [72, eqs.(6–7)], neutral/ionised targets [48, §VI.] or atoms/molecules [46]. We will only mention the two following semi-empirical approximations:

Burgess denominator : proposed by Vriens [89] when taking into account that the orbital electron bound by B_j has a kinetic energy $U_j \equiv \langle p_j^2/2m_e \rangle$ corresponding to its average squared kinetic momentum.

$$K_j = (U_j + B_j)/n_j . \quad (2)$$

The kinetic energy term U_j emerges as we average on the bound electron's orientation in the binary-encounter model. The division by the principal quantum number n_j was added later in Huo and Kim [35, §III.B:p.1234] as a correction for ionisation from outer shells of heavy nuclei ($n_j \geq 3$) [for atomic targets].

Screening correction : proposed by Guerra et al. [28] in order to replace a tentative modification of the BEB scaling for inner-shell ionisations by Santos et al. [72, eq.(6)]. Their new formula reads as:

$$K_j = 2\text{Ryd} \left(a \frac{Z_{\text{eff},n\ell j}}{2n^2} + b \frac{Z_{\text{eff},n'\ell' j}}{2n'^2} \right) . \quad (3)$$

The effective nucleus charge Z_{eff} is obtained from the data of Clementi and Raimondi [13] as $Z_{\text{eff},1s} = 0.9834Z - 0.1947$, $Z_{\text{eff},2s} = 0.7558Z - 1.1724$ and $Z_{\text{eff},n\ell j} = Z - \sum_{i=1}^{n-1} 2(i-1)^2 - 2\ell^2$ otherwise. The full screening is a linear combination (set as $a = 0.3$ and $b = 0.7$) between the effective screenings of the current ($n\ell$) and the next occupied ($n'\ell'$) subshells (higher in energy). Note that for the valence subshell, the model sets: $n'\ell' = n\ell$. Additionally, for molecules, the principal quantum number n is not a good number and may be used only on inner (non-valence) orbitals.

Both expressions try to estimate the kinetic energy K_j of the incident electron at the place where ionisation takes place. Obviously, this classical view of ionisation

has limitations; as the dominant dipole interaction is of long range and thus one may not “locate” the incident electron. Nevertheless, formally, one may say that the BEB model relies on the first (plane wave) Born approximation, which is known to always overestimate the interaction, since it does not consider distortion of the incident electron wave due to the potential of the target. The K_j kinetic energy may thus be formally considered as an effective correction to the incident electron energy due to its distortion in the potential (including correlation with bound electrons) throughout the whole interaction. Further discussion on this scaling may be found in Tanaka et al. [85, §B.1.a] and references therein.

Since the purposes of the two scalings defined above are complementary, in section-4 we will use eq. (2) for valence shells and eq. (3) for core $1s$ shells (whether atomic or molecular) in the following study. In any case, the estimation of K_j , whether it stems from a binary-encounter approximation as in eq. (2) or a screening estimation as in eq. (3), is independent from the intervention of the ionisation threshold I_j in the bracketed term of eq. (1).

2.2. The dipole oscillator strength

The assumption c) on the sum of the dipole oscillator strength density calls for a more detailed explanation. In the Bethe theory of inelastic collisions, the asymptotic expressions of both integral electronic excitation and ionisation cross sections are found to be proportional to a quantity named as the dipole oscillator strength and noted f [39, eqs.(4.18),(4.29)]:

$$\sigma_{\text{exc},j} \sim \frac{f_{\text{exc},j} \text{Ryd}}{W_j} \frac{\ln \varepsilon}{\varepsilon} + O\left(\frac{1}{\varepsilon}\right), \quad (4)$$

$$\sigma_{\text{ion},j} \sim M_{\text{ion},i}^2 \frac{\ln \varepsilon}{\varepsilon} + O\left(\frac{1}{\varepsilon}\right). \quad (5)$$

The labels j, i are mere indexes for different discrete excitations and ionisation channels respectively. The quantity W_j is the energy threshold for an electronic excitation indexed j . The electronic excitations for which $f_{\text{exc},j} > 0$ are qualified as (optically or dipole) *allowed*, whereas the rest are *forbidden* and their asymptotic behaviour on the kinetic energy of the primary electron ε falls faster ($\sim 1/\varepsilon$ or steeper).

The quantity $M_{\text{ion},i}^2$ (known as the “dipole-matrix-element squared”) is an integral over the kinetic energy of the secondary electron w from the ionisation channel i , obtained with the *differential* (or density) dipole oscillator strength [85, eq.(19c)]:

$$M_i^2 = \int_0^\infty \frac{\text{Ryd}_i}{w + I_i} \frac{df_{\text{ion},i}}{dw} dw. \quad (6)$$

In addition to the Bethe approximation, the assumption b) above of the BEB devises a profile for the dipole oscillator strength density as [48, eq.(46)]:

$$\frac{df_{\text{ion},i}}{dw} = \frac{N_i I_i}{(w + I_i)^2}, \quad (7)$$

where N_i is the integral value of the oscillator density. Then, in the BEB, the value $M_{\text{ion},i}^2$ equals $N_i \text{Ryd}/2I_i$ [48, eq.(49)].

The dipole oscillator strengths (and their integrals) are all linked and constrained by an equation known as the Thomas-Kuhn-Bethe sum rule and amounting to the total number N of electrons bound by the target (atom or molecule) [85, eq.(16)]:

$$\sum_j f_{\text{exc},j} + \underbrace{\sum_i \int_0^\infty \frac{df_{\text{ion},i}}{dw} dw}_{\equiv N_i} = N. \quad (8)$$

Finally, the BEB's assumption c) on the Thomas-Kuhn-Bethe sum consists in setting $\sum_i N_i = N$ [48, eq.(49) with $Q = 1$], and henceforth $\sum_j f_{\text{exc},j} = 0$.

Of course, this is not the case in practice and therefore this implies that the BEB should, in principle, asymptotically tend to overestimate the total ionisation cross section since it is encompassing all optically allowed excitations; whether they actually lead to ionisation of the target (like autoionisations) or not. In this way, we note that the BEB includes optically allowed autoionisations *implicitly* (through the contribution of their dipole oscillator strength which affects the asymptotic region).

Notwithstanding, if we consult the various targets onto which the BEB has been applied, we do not observe any asymptotic overestimation. Indeed, the cyan curves on figure 4 below reproducing the original total ionisation BEB cross sections align generally well with the experimental data. The examples matching best are N, CO, N₂, O₂, CO₂ and NO₂.

Asymptotically, the values at a few hundreds of eVs should not be affected by the scaling K_j which, for the targets selected, stays $\lesssim 100$ eV for ionisation from the valence shell accounting for most of the total cross section. Therefore, we surmise that this unexpectedly good agreement stems from the last assumption: namely the Hartree-Fock modelling of the target.

2.3. The Hartree-Fock orbitals

The total ionisation cross section of the BEB is constructed as a sum of ‘‘orbital’’ cross sections :

$$\sigma_{\text{tot}}(\varepsilon) = \sum_{j=1}^{n_{\text{orb}}} \sigma_j(\varepsilon), \quad (9)$$

Such denomination was proposed by the original authors, because these σ_j (1) are based on the theoretical orbital structure of atoms or molecules in the Hartree-Fock approach where each electron is bound to its orbital j by a theoretical binding energy B_j . Additionally, only the lowest binding energy was replaced by its experimental value, so that the total cross section have a threshold consistent with experiments [36, p.2966].

Such decomposition of σ_{tot} , however, is artificial and may not be used to estimate the sub-processes of ionisation from individual orbitals. This was well pointed out in Hwang et al.'s conclusion [36, p.2966]:

[the BEB model] can be used – for the total ionization cross section, not orbital cross sections –

There are two reasons for this inadequacy:

- (i) The Hartree-Fock model has its limitations and does not incorporate accurately the correlation forces between bound electrons. As a result, the Hartree-Fock values of the binding energies B_j may differ significantly from experimental measurements I_j [19, table 1]. This was used to point out some shortcomings of the Hartree-Fock approximation and molecular orbital theory for predicting the ordering of molecular orbitals binding energies [e.g. for N_2 : 10].
- (ii) The modelling of ionisation as a removal of an electron in an occupied orbital relies on the so-called generalised Koopman or “frozen orbital” approximation. The generalised Koopmans [51] approximation states that the binding energy B of an electron in a Hartree-Fock atom/molecule described by a single Slater determinant is equal to the ionisation threshold I of that atom/molecule for the removal of that electron. Usually, a single Slater determinant is not sufficient to properly describe an atomic or molecular state. But the greatest error induced by the Koopmans approximation is to picture the removal of an electron meanwhile the other electron orbitals remain “frozen”; i.e. that they do not relax upon the disappearance of a bound electron [79, §5:p.53].

In brief, Hartree-Fock and Koopmans approximations do not accurately represent the correlation between bound electrons. After examination, we realised that the theoretically calculated orbital binding energies using these approximations are generally overestimating the experimental ionisation thresholds: $B_j \gtrsim I_j$. As a result, the total BEB cross sections when using the theoretical B_j are roughly proportionally lower than they would be using the experimental I_j (because the magnitude factor in eq. 1 $\propto 1/I_j$). Furthermore, the Koopmans approximation misses out an important aspect of partial ionisation processes: that removal of an electron from a concrete orbital actually opens up to a variety of ionisation channels, each at a different ionisation threshold.

In the present paper, we propose a decomposition of the BEB (shown in table 1) into cross sections associated to specific ionisation channels with *experimental* values of ionisation potentials I as identified in photoelectron spectroscopy [79]. In the next section, we introduce what such ionisation channels are.

3. Ionisation channels

From the discussion above, we know that having the BEB rely on the Koopmans approximation is restrictive because ionisation to an excited ionic state does *not* merely correspond to the removal of an electron from an occupied orbital. To model accurately the underlying complexity of the ionisation process is a very difficult task. Ideally, one should aim to a complete description of all the processes that can be identified in the photoionisation spectrum – and therefore participate in the dominant dipole

term of the electron impact ionisation. Nonetheless, semi-empirical models, such as the BEB have proven to be simple yet fairly accurate representations of the *total* ionisation cross section. We argue hereby that *partial* ionisation to excited ionic states should be modelled in the BEB model with regard to the ionisation peaks or more generally the prominent features observed experimentally through photoionisation spectroscopy [80]. In this way, the application of the BEB model does not need to restrict itself only to targets for which the lower cationic states are well described by the removal of a single electron from the ground state configuration built from Hartree-Fock orbitals.

Generally speaking, ionisation induces a perturbation on the orbital structure of the ion which we may exemplify in three types of situations:

- a) Coupling: for open-shell targets, ionisation from a closed subshell leads to different coupling possibilities of the orbital and spin moments with the electrons in the open shell. For instance, ionisation from the $2s$ orbital of the carbon atom can lead to a 4P , 2D , 2S or 2P ionic C^+ state. Another example is illustrated by the warmly (orange, yellow, brown) coloured lines of different stroke patterns representing the states ($^4S^o$, $^2D^o$, $^2P^o$) of ionised atomic oxygen after ejection of a ($2p$) electron on the top graph of figure 1.
- b) Reallocation: some of these states (the doublets) may only result from a subsequent reallocation of electrons in the orbitals of an open subshell ($2p$). The metastable singlet states of $N^+ ^1D$ and 1S are other good examples, which require that one of the two remaining electrons in the $2p$ orbital (after ionisation) flip its spin projection. A change in electron spin is most probably due to exchange with the incoming electron [78, p.11] though (rather than a spin-flip interaction).
- c) Shake-up: at high incident electron energies, it is possible that, in addition to ejecting an electron from its orbital, other electrons from the valence shell be excited to other orbitals. In X-ray photoelectron emission, this is known as “shake-up” [79, p.26]. An example of “shaken-up” ionic states are the $B ^2\Sigma_u^+$ and $C ^2\Sigma_u^+$ states of N_2^+ which are configuration mixtures between a removed $2\sigma_u$ electron and an excited electron in the $1\pi_g$ orbital [60].

The connection between *photoelectron* spectroscopy and electron impact ionisation is established by the dipole oscillator strength in the Bethe theory. We thus expect that states responsible for prominent bumps in photoionisation spectra will also have important contributions in impact ionisation cross sections. Conversely, weak features will remain negligible. Below, we discuss how we can adapt the BEB model to take into account the aspects aforementioned.

Ionic state multiplicity. In light atoms, the break of degeneracy in the energy levels from the Russell-Saunders LS coupling is very weak. As a consequence, the relative contribution of ionisations to excited ionic states from the same valence subshell were proposed by Kim and Desclaux [47] to be weighted by the statistical multiplicity of the ionic states. For a state labelled as ^{2S+1}L (e.g. $O^+ ^4P$

with $S = 3/2$ and $L = 1$) the multiplicity m_p is given by $(2S + 1)(2L + 1)$. These statistical weights rely on combining initial states which can be treated as degenerate at incident electron energies much higher than the respective partial ionisation thresholds (away from resonances and couplings) and only among ionic excitations which involve the same degree of interaction (dipole-allowed, spin-forbidden, etc.) [67, p.12]. Thus, the parameter N becomes a ‘‘participation’’ weight of electrons in the channel (rather than the number of electrons on an occupied orbital). For molecules, N is weighted likewise according to the multiplicity of each final ionic state. One can consult the values of N that we calculated for various ionisation channels in table 1 at the end of this article.

Spin-forbidden ionisation channels. When evaluating the participation weight N , one must also be cautious of whether the ionisation involves flipping of an electron’s spin. Ionisation events accompanied by a change of electron spin in the occupied orbitals, are analogous to optically spin-forbidden excitations except that they are accompanied with an emission of an electron in the unbound continuum. They do not participate in the Thomas-Kuhn-Reich-Bethe sum rule as their differential oscillator strength distribution should be zero. This implies that such ionisation channels will not be visible on photoelectron spectroscopy and consequently, we can expect that the cross sections by such ionisation events be small compared to optically-allowed channels.

Accurate B-spline R -matrix calculations by Wang et al. [91] of spin-forbidden ionisations from N^4S to N^+^1D and 1S show that they contribute to less than 1 % of the total ionisation. Given the fact that spin-forbidden excitations have an asymptotic decay at $\sim 1/\varepsilon^3$ [39, p.341:left column], we expect spin-forbidden ionisations to have a similarly steep decay. In the BEB model, this minor contribution may only come from higher order terms (steeper than $O(1/\varepsilon)$ in equation 5) than that of the dipole oscillator strength. Given their rarity of occurrence, we shall dismiss these contributions to total ionisation. We will comment more on this case in section 4.1 when we assess the BEB for atoms.

Vertical ionisation thresholds. Moreover, if the target is a molecule, its bond length and molecular shape may significantly change after being ionised. A notable example is the nitrogen dioxide (NO_2) which, upon removal of its singlet ($6a_1$) electron, changes to a linear $^1\Sigma_g^+$ equilibrium geometry [5, p.452] as its isoelectronic CO_2 molecule. Thus, molecular ionisation induces also a vibrational transition for which we have to distinguish the adiabatic energy threshold from the vertical (peak) energy threshold as explained in Siegbahn et al. [79, p.55]. In this paper, following Kim et al.’s conclusion [46], we always use the *vertical* ionisation threshold.

Autoionisation. For resonances, the BEB model actually accounts for the oscillator strength due to dipole-allowed excitations leading to autoionisation, so that their contributions are tacitly included (see section 2.2). This is because the BEB was obtained assuming that the Thomas-Kuhn-Bethe sum of the oscillator strengths is

entirely due to ionisation[48]. As for autoionisations from dipole-forbidden excited states (thus absent in the photoelectron spectroscopy), their decay, as the incident electron energy grows, is much steeper than from dipole-allowed states; so their overall contribution is restricted to a small resonant region.

Branching ratios. The complexity of the ionisation process implies also that there is not only one way to produce specific ionic species. Apart from direct ionisation, ions can also be produced by autoionisation. Multiply excited ions can be formed by shake-off (interaction with more than one electron) or Auger emission subsequent to a core ionisation (which, in light atoms, is more common than X-ray deexcitation [80]). However, the experimental cross section for production of multiply charged ions starts at a much lower threshold than the binding energy of a $1s$ electron and is also significantly larger than ionisation from the K-shell (fig. 2). Thus, multiple ionisation mechanisms are mostly imputable to complex electron-ion interaction beyond the single binary-encounter model and subsequent autoionisation. In molecules, double ionisation almost always leads to a ‘‘Coulombic explosion’’ whereby energetic atomic ions are ejected apart [7, p.155–157]. Because of the multiple possible processes subsequent to ionisation to an excited state in molecules, one requires *branching ratios* to estimate the production of an ion fragment from a particular ionisation channel. Such endeavour was already undertaken in other studies [34] and will not be covered here.

In light of this correspondence analysis between the BEB model and ionisation processes, we proceed in the following section to the application of experimental thresholds determined from photo-ionisation spectra as input parameters to the BEB model and comment on the result.

4. Application

We now apply the separation of the BEB model into partial ionisation channels from the valence shell and from core orbitals to four light atoms: C, N, O, F; four diatomic molecules: CO, N₂, O₂, NO; and four triatomic molecules: CO₂, H₂O, NO₂ and O₃; all which are of interest in cold plasmas in atmospheric gases. The identified processes are gathered in table 1 together with:

- I : the corresponding experimental ionisation potentials from photoelectron spectroscopy;
- K : scaling factors calculated with:
 - eq. (2) for valence-shell orbitals using experimental ionisation thresholds for ‘‘binding energies’’ ($B = I$) and kinetic energies U from Kim and Desclaux [47] (C,N,O atoms), Hwang et al. [36] (diatomic), Kim et al. [46] (triatomic) and from the orbital wavefunctions of Koga et al. [50] (fluorine);
 - eq. (3) for the core $1s$ shell;

- N : participation of electrons in each channel, as mentioned above, according to the multiplicity rule of the final ionic state $(2L + 1)(2S + 1)$ and the electron occupation in the corresponding orbital. Contributions from spin-forbidden reactions (displayed for comprehensiveness and noted with a barred arrow \rightarrow) are assumed negligible.

The last column gives the references from which the ionisation channels and their thresholds were extracted.

The BEB model with all identified partial ionisation channels is illustrated in figure 1, for an atomic (O), diatomic (NO) and triatomic (O_3) gaseous target. Each line is associated to (a.) the ejection of an electron from an orbital (in the Hartree-Fock picture) or to (b.) an ionisation channel (in the more general picture). Different partial cross sections due to ionisation from the same orbital are represented with different line styles (solid, dashed, ...). Lighter colours are used for outer shells/smaller binding energies. We can observe the influence of the ionic multiplicity on the predicted partial ionisation cross section, and therefore a separation in magnitude between groups of different multiplicities as we see by the triplet and singlet ionic excitations of NO (middle graph).

For better visibility, partial ionisations from the 1s (K) shell are displayed on a separate graph in figure 2, where we stacked ionisations from C, N and O atoms according to the slightly varying 1s binding energies in different molecules. The greatest differences arise from 1s electrons bound to carbon in methane (CH_4) which was used in the experimental study of Tawara et al. [86]. These experimental data were reported as X-ray production cross sections and require the fluorescence yield ω_{1s} in order to convert into impact ionisation cross sections. On this issue, note that the experimental K-shell cross sections displayed on Santos et al. [72, fig.1] for N are lower than in Llovet et al. [59, fig.11:p.46] using fluorescence yields reported in the EADL [66]. For disambiguity, in the caption to our figure 2, we specified the fluorescence yield ω_{1s} that we used.

Aware of the inadequacy of the original BEB model for ionisation from core shells, Santos et al. [72, eq.(6)] proposed to patch the model with an empirical averaging of the scaling factor, the result of which is reproduced in grey solid curves. Overall, the K estimated by screening eq. (3) gives a better agreement than the empirical averaging of Santos et al. [72, fig.1–2]. The slightly worse agreement for O is subject to debate on the value of the fluorescence factor used to convert the X-ray yield into cross sections. Additionally, we deem that the disagreement at energies near threshold is due to loss in accuracy of experimental results, since they [86] give non-zero values at energies below the ionisation threshold identified in photoelectron spectroscopy. Therefore, we advocate that the BEB model be used with K as a parameter tabulated as we do so in table 1, rather than to rely on semi-empirical formulas based on other parameters (such as the kinetic energy U of bound electrons). It would be challenging to find a universal analytical formula for K . On the other hand, we do not oppose proposals of calculating K *ab initio*, such as from the average ratio between cross sections from the plane wave and the distorted-wave approximations.

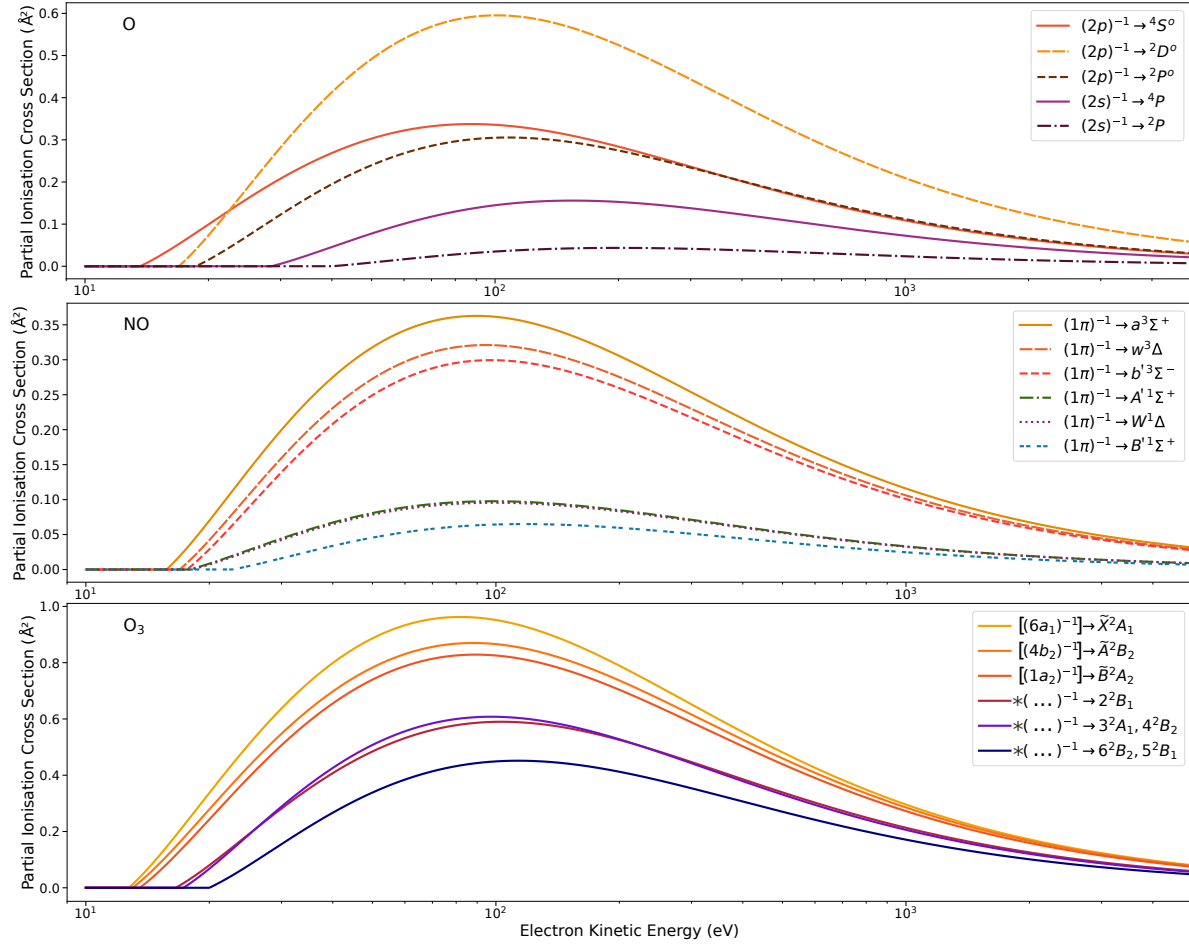


Figure 1. Partial ionisation cross sections obtained with the BEB model for atomic oxygen (top), nitric oxide (middle) and ozone (bottom) with parameters reported in table 1. Lighter colours are associated to outer orbitals (lower binding energies). Different line styles distinguish ionisations corresponding to a removal of an electron from a same orbital but with different ionic outcomes. Coupling between momenta of unpaired electrons leads to different ionic states whose multiplicities reflect their intensity as in atomic oxygen and the triplets and singlets in nitric oxide. The orbital picture does not apply well to ozone. Although the first three ionic states may still be identified with electron ejection from an orbital with a leading configuration [in square brackets], ionisations from deeper valence orbitals (*) may only be identified with final ionic states whose many vibrational bands overlap over a certain region in the photoelectron spectrum, and which are bundled together to form the “partial” impact ionisation cross sections drawn on the bottom graph.

When comparing with the original BEB model based on Hartree-Fock binding energies, one must recede to the removal from an orbital picture, and add all ionisation channels which originate from the same orbital. In figure 3, one can see clearly that, for the three targets selected (N, O₂ and CO₂), all theoretical binding energies overestimate the experimental ones (the thresholds of dashed lines are all at higher energies than of solid lines of the same colour). As a direct consequence, the partial cross sections resulting from theoretical binding energies are scaled down compared to our newly

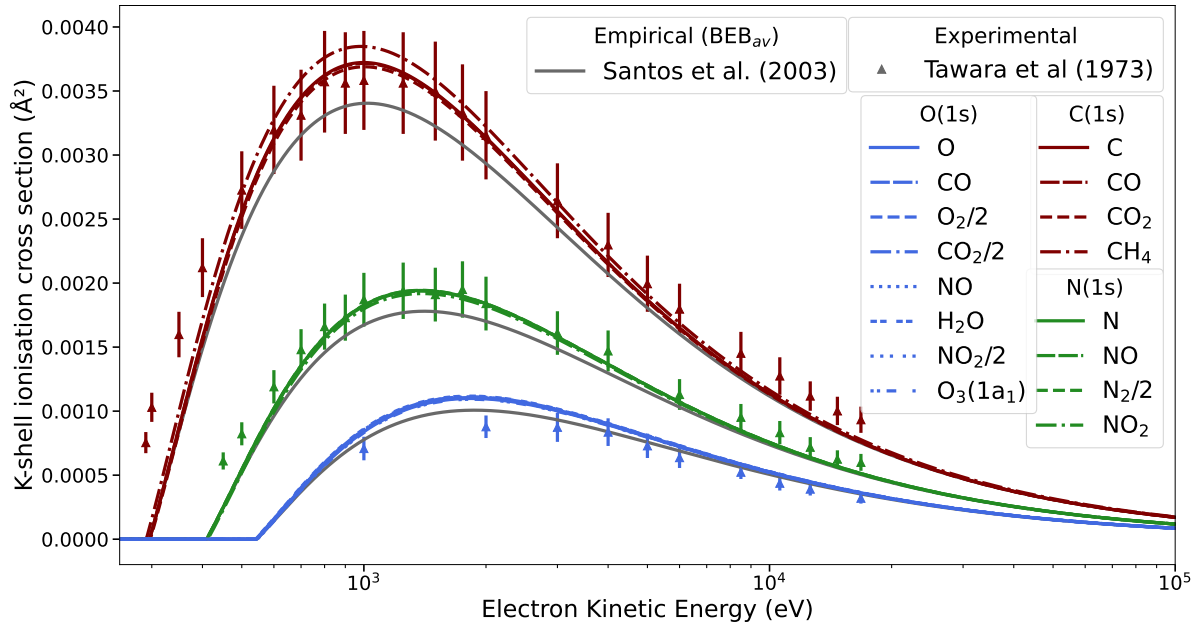


Figure 2. Partial ionisation cross sections from the 1s shell of C, N and O atoms in their free form and bound in various molecules. The 1s binding energies I are reported in the first rows of table 1 for each gaseous element. The scaling energy K is calculated with eq. (3). Fluorescence factors used to convert experimental data are from Tawara et al. [86]: $\omega_{C_{1s}} = 2.47 \times 10^{-3}$ [37, table I], $\omega_{N_{1s}} = 4.35 \times 10^{-3}$, $\omega_{O_{1s}} = 6.91 \times 10^{-3}$ [58] (see main text for explanation).

calculated ones.

Finally, the total ionisation cross sections (in solid red), obtained as a sum of all the partial cross sections such as those presented in figure 1, are compared to experimental total ionisation cross sections in figure 4. The success of the BEB model in reproducing the *total* ionisation cross section was already well established in a series of publications [36, 46–48]. Nevertheless, yon calculations (reproduced in solid cyan lines) relied on theoretical Hartree-Fock orbital binding energies which do not concord with the experimental thresholds for ionisation to excited states. The current figure 4 shows that for some targets, good agreement can be preserved when using experimentally determined ionisation thresholds. For other targets, the BEB model ceases to give an accurate representation of the total ionisation cross section implying that a further scaling is necessary.

Below, we comment on the total and partial cross sections of ionisation obtained for each of the targets considered. Based on information available in the literature, we explain how we identified each of the ionic states and whether these may be considered as pure states with holes or mixtures.

4.1. Atoms

Overall, the agreement of the sum of BEB partial cross sections with experimental data from atomic targets is good, except for fluorine. On left column of figure 4 we

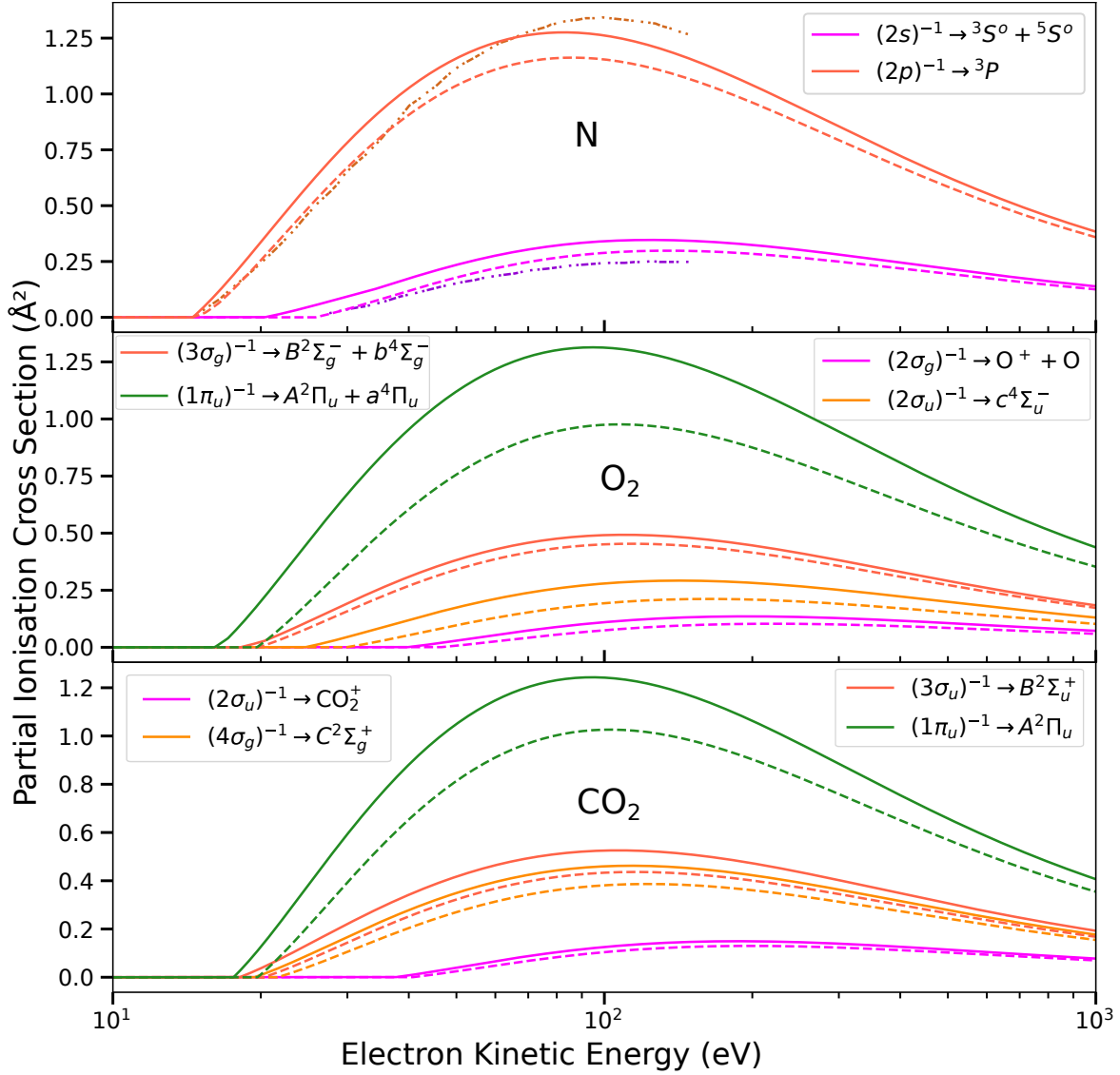


Figure 3. “Orbital” ionisation cross sections obtained with the BEB model for atomic nitrogen (top), molecular oxygen (middle) and carbon dioxide (bottom). Solid lines (—) show the sum of partial cross sections from ionisation channels associated to removal from a molecular orbital with parameters reported in table 1. Dashed lines (---) of the same colour correspond to original BEB model with theoretical thresholds from Hartree-Fock calculations. The shattered lines (\cdots) show the BSR calculations for N from Wang et al. [91, figure 7]. Higher ionisation thresholds directly imply roughly proportionally lower cross sections as can be identified from eq. (1). This difference remains on the total ionisation cross section in fig. 4.

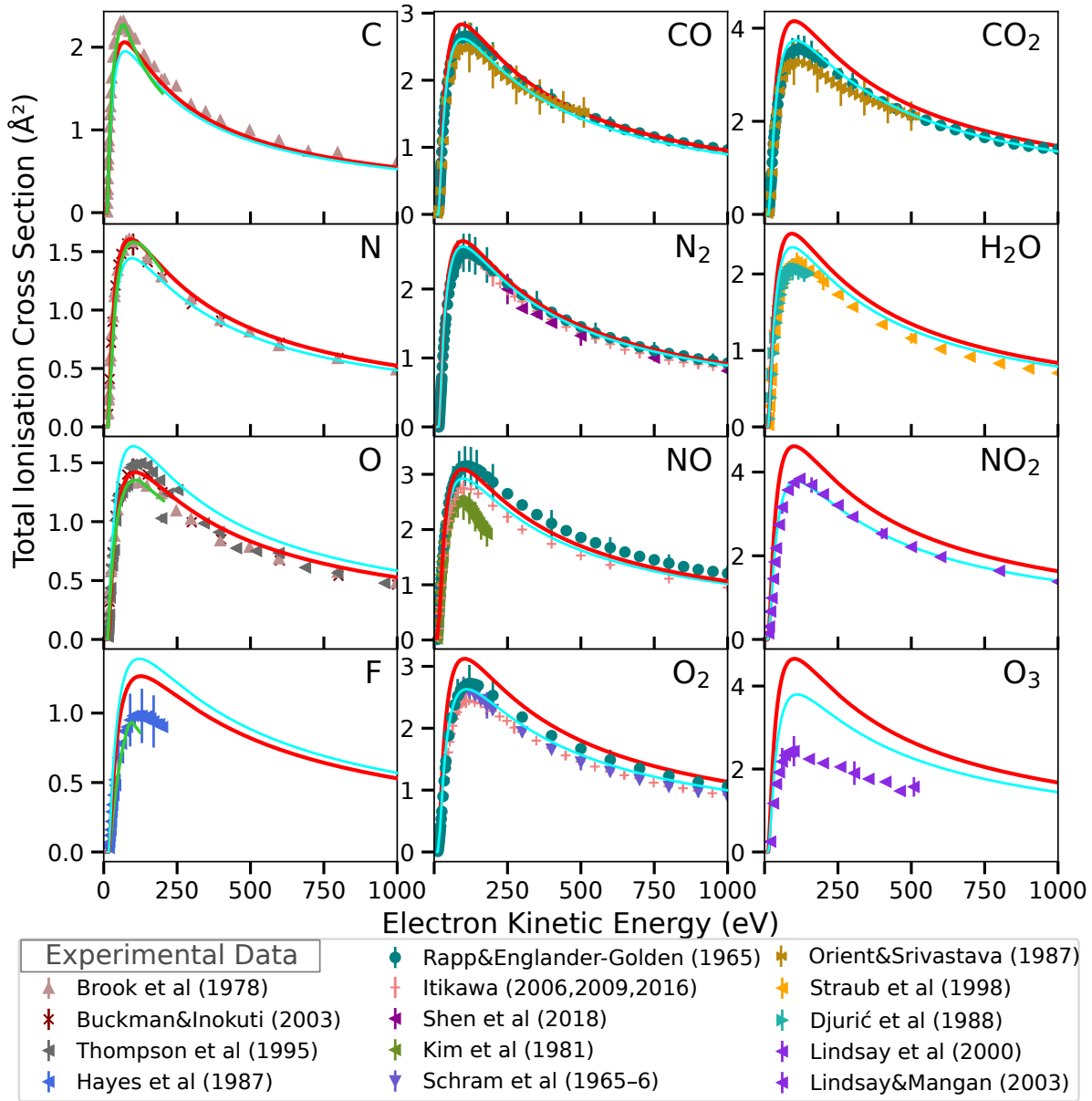


Figure 4. Sum of partial ionisation cross sections from the BEB model with experimental ionisation thresholds I (table 1) in red solid (—) and original Hartree-Fock theoretical binding energies in cyan (—) compared with experimentally measured total ionisation cross sections for four atoms, four diatomic and four triatomic molecules. For atomic targets (left column), BSR calculations are shown in light green (—) from [26, 87, 90, 91]. Experimental data are from [2, 8, 18, 25, 30, 38, 40–42, 45, 56, 57, 64, 65, 68, 69, 74–76, 83, 88]. The alignment of the source labels echoes the 4×3 grid, although some sources give data for many different targets.

also display the BSR calculations from Zatsarinny and Bartschat [94] in light green. It is worthwhile to mention that in the experimental measurements of Brook et al. [8], metastable excited atoms entered the collision chamber. However, the data used in our plots is the corrected cross sections after subtracting the extrapolated signal from these metastable states (whose ionisation threshold is lower than the ground state). Therefore, we cannot exclude that some discrepancies might be also due to inaccuracy of the experimentally derived cross sections.

C. When it was first modelled with the BEB, Kim and Desclaux [47, fig. 1] argued that the shortcomings of the BEB ionisation cross section could be compensated by including contributions from autoionisations. While we do believe that this assumption might be correct, we argue that, before adding autoionisations, one ought to first subtract the part of the oscillator strength imputable to autoionisations from the BEB model. Indeed, the asymptotic form of the separately calculated autoionisation (ai) cross sections follows $\sigma_{\text{ai}} \sim f_{\text{ai}} \ln \varepsilon / \varepsilon$. Then, it follows from the discussion in section 2.2, that the dipole part of the BEB should be scaled as $(N - f_{\text{ai}})/N$.

In practice, this means to replace the BEB model by the so-called “BEQ” model where the Q parameter plays the role of the (normalised) Bethe sum. This would lower the corresponding BEQ cross section, but since our newly calculated cross section (red solid line on fig. 4) is larger than the previously used BEB, the scaling down by Q could then make the two (solid red and cyan) curves match and preserve the agreement seen on Kim and Desclaux [47, fig. 1]. Nonetheless, Wang et al. [90, p.6 left] argue that this agreement is fortuitous due to an overestimation of the oscillator strengths used for the autoionising states. This should be verified in a more detailed study incorporating the dipole oscillator strengths which is beyond the scope of the present study (limited to the pure BEB model).

For partial ionisations from the K-shell (fig. 2), we used the experimental data of the 26th line reported in table IV of Bruch et al. [9] and added the ionisation potentials (CI \approx 11.26 eV and C II \approx 24.383 eV) reported in the NIST database [52]. Guerra et al. [28], Santos et al. [72] extracted their data from the same source, but we lack information about how the numerical value of the binding energy was derived.

N. The situation is similar to carbon; updating the thresholds raises the total BEB cross section. This casts doubt on the previous conclusion that Brook et al.’s *adjusted* experimental data [8, table 5] is notwithstandingly plagued with 30% of N^2D as suggested in Kim and Desclaux [47, fig. 3]. We have two strong supporting reasons to claim that this was not the case:

- i. The experimental data of Brook et al. [8, table 5] is *already* accounting for the spurious signal from metastable species. From their measured cross section (“ Q_m ”), they subtracted ionisation from metastable states using an “apparent” cross section Q_a^* extrapolated with a simple power-law “constant/ ε ”, and obtained thus a “true”

cross section Q (reported in the middle column of their tables). While it is not sure how crude that estimation is, when comparing with experimental data, Kim and Desclaux [47] ought to have used the measured cross section Q_m and not the corrected cross section to validate their argument about the mixture of metastables (from our close examination of their figure, it seems that they have used the adjusted value $Q(E)$ in [8, table 5]).

- ii. The original cross section of Kim and Desclaux [47] (cyan fig. 4) is low because they statistically weighted total ionisation to two spin-forbidden ionisation channels namely: $(2p)^{-1} \rightarrow N^{+1}S$ (18.59 eV) and $(2p)^{-1} \rightarrow N^{+1}D$ (16.43 eV) higher than the ionisation from ground channel at 14.53 eV. Later, B-spline calculations from Wang et al. [91] found out that the contribution from the aforementioned spin-forbidden ionisation channels is negligible ($> 1\%$). As a result, they obtained a larger ionisation cross section from the 2p orbital than we did.

A comparison of ionisation channels from 2p and 2s orbitals of BEB is given on the top graph of figure 3 where we show additionally in shattered linestyle the BSR calculations from Wang et al. [91, fig. 7].

(2p)⁻¹: The BSR results are closer to the BEB with original thresholds (with statistical weighing to forbidden-states included) at energies up to 50 eV, but then the BSR calculations exceed the BEB model even with updated thresholds. Assuming that the BSR calculations are accurate, that would mean that the BEB would need to have its scaling (K) revised as in eq. (2 since it is effective only at energies near threshold.

(2s)⁻¹: The BSR does not have the same threshold as the one we found for $N^+(2s2p^3)^3S^o$ at 20.34 eV from the NIST database [52]. This results in a higher BEB cross section compared to the BSR. Further clarification would be needed in order to understand why the thresholds do not concord.

In the meantime, we extend Wang et al.'s critique of the BEB results, by stating that the model needs revision on the thresholds used and the ionisation channels open.

O. For oxygen, we are unable to reproduce the original BEB from Kim and Desclaux [47] because they did not disclose the thresholds used to generate the two metastable ions $O^{+2}D^o$ and $O^{+2}P^o$. When we use our thresholds, we obtain the red solid curve on figure 4 which already overestimates the cross section in the asymptotic region and does not underestimate it below 100 eV to the extent observed on [47, fig. 4]. Once again, we do not deny that atomic oxygen has several autoionisation channels, but if these are to be included separately, the BEB must be downscaled according to the part of the dipole oscillator strength taken by these autoionisations (same argument as for carbon). The BSR calculation digitised from Tayal and Zatsarinny [87] reproduces well the measurements of Brook et al. [8]. The authors argued that differences of the BEB with BSR is due to the modelling of autoionising excitations.

F. For fluorine, the overestimation of the cross section results from a too large optical oscillator strength of the ionisation channels. Overall 12% of the Bethe sum is taken by discrete excitations [26, table II]. Then, better results can be obtained when a more accurate model of the dipole oscillator strength is used [8, 48, §3.2, fig. 9]. Although it seems that fluorine lies beyond the applicability of the BEB model, BSR calculations from Gedeon et al. [26] agree well with the experimental data of Hayes et al. [30].

4.2. Diatomic molecules

Except for O₂, the difference on the total ionisation cross section between the original and revised BEB is minor, while the thresholds can differ by 10%. For each molecule below, we discuss the various ionisation channels identified in relationship with the orbital structure and the likelihood of dissociating after ionisation. Where possible, we provide information on branching ratios of dissociation and predissociation of molecular ions obtained from elastic photoionisation cross sections. In general, the yield of doubly ionised whole molecules (which depends also on their lifetimes), though non-zero, is negligible compared to dissociation into ionic fragments [56, p.5-20,63].

N₂. The two closed-shell and isoelectronic molecules are N₂ and CO. They are the simplest to describe in terms of removal of an electron from a molecular orbital, although the B and C states of N₂ are not pure states but different configuration mixtures with an excited $2p\pi$ electron [60, table 1]. The C state predissociates from the vibrational level $v' \geq 3$ [23]. Removal of a $2\sigma_g$ electron most likely dissociates into N+N⁺, whereas a hole in the core orbital provokes an Auger emission followed by a separation into N⁺+N⁺ [7, p.216]. A comparison with the partial ionisation cross section for N⁺ fragments of Straub et al. [82] would reveal that there is a significant portion of N⁺ currently unaccounted by theoretical predictions from ionisation channels. These could come from a post-collision interaction of a secondary electron emitted from the $2\sigma_u$ orbital, whose energy is high enough to excite the nitrogen ion beyond its dissociation limit at 8.7 eV as suggested by photoelectron spectroscopy [79, p.64].

CO. Presently, carbon monoxide is the only diatomic molecule for which we maintained a one-to-one correspondence between ionisation channels and ejection from molecular orbitals (see table 1). Thus, the lifting of the red from the cyan curve on top of figure 4 comes from a reevaluation of the higher ionisation thresholds whose former overestimation rated roughly 10%.

Nonetheless, above the B²Σ⁺ state (ejection of 4σ electron), the excited ionic structure becomes more complex and there are many weakly bound states which predissociate into C⁺+O fragments [7, p.229]. These cannot be simply modelled in the bound-orbital structure as presented here. The details about dissociation paths ensuing the removal of a 3σ electron is subject to discussion. From ionisation of core orbitals, the yield in atomic carbon and oxygen ions is assumed to be roughly equal.

NO. Due to having a single 2π electron, nitric oxide has the most diverse array of excited ionic states. Six states (three singlets and three triplets) may be formed by removing one 1π electron due to the different coupling possibilities with the lone 2π electron [32, table I]. This separation into singlet and triplets can be observed as two groups of orange curves on the partial cross sections represented on figure 1–middle graph. The labelling of the highest lying $B^1\Sigma^+$ singlet requires confirmation [33, p.482].

NO is a good example to show that, when the Hartree-Fock calculated binding energy (18.49 eV [36, table 1]) of an orbital (1π) lies somewhere in the middle of a more complex subdivision of ionisation channels ($\in [15.73; 22.73]$ eV), the difference in the total ionisation cross section between original (cyan) and revised (red) BEB remains smaller than for CO as observed on figure 4; despite the fact that there is a qualitatively greater difference between the original and revised modellings of NO than for CO.

The energy range of the different states with a hole in the 1π orbital overlaps with the states with a hole in the 5σ orbital. Therefrom, one can find a different ordering of these orbitals (5σ and 1π) according to their “binding” energy when the electronic configuration of NO is presented in the literature (e.g. compare Berkowitz [7], Hwang et al. [36, p.231,table I] versus Huber [32]). Since, the vibrational bands of some of the $(1\pi)^{-1}$ and $(5\sigma)^{-1}$ states overlap, they can be pragmatically grouped together under a common binding energy, but with different relative contributions [21].

Next, the two higher ionic states c and B coming from removal of a 4σ electron are actually suspected to be mixtures with a $(2\pi)^2$ configuration [55]. In any case, they predissociate predominantly into $N^+ + O$ [7, p.236]. Also, there are indications that removing a 3σ electron also favours a $N^+ + O$ dissociation [7, p.237], though we do not know whether the states are repulsive or weakly bound and predissociate.

O₂. Molecular oxygen has a partially occupied $1\pi_g$ orbital and, as a result, ionisation from inner subshells can either produce quartet or doublets [7, p.219]. The improper ordering of the $1\pi_u$ and $3\sigma_g$ orbital energies of the Hartree-Fock model [36, table 1] is responsible for the significant overestimation of the corresponding ionisation threshold (green solid and dashed lines on the middle graph of figure 3) and explains the major difference in the total ionisation cross section between original and revised BEB.

Predissociation of oxygen starts from the $v' \geq 4$ of $b^4\Sigma_g^+$, but is weak. It becomes stronger for the B state and the $c^4\Sigma_u^-$ can be considered to predissociate completely [7, p.222]. Whereas ionisation from the core orbitals leads to Auger emission and dissociation, removal of a $2\sigma_g$ electron can both lead to formation of a very high-lying (bound) doublet state or a dissociating (repulsive) quartet state. There exist a series of excited ionic states which stem from more complicated configurations.

4.3. Triatomic molecules

Overall, the overestimation of the total ionisation cross section for triatomic molecules is worse than for diatomic ones (where the revised BEB model still gives very reasonable

estimation).

CO₂. Carbon dioxide is the only linear triatomic molecule, the others (in their ground state) belong to the C_{2v} symmetry point group [see 31, §4.3.2]. A good summary of carbon dioxide's properties and electronic structure is available in Aresta et al. [3, §1.2]. Similarly as for CO, the difference of the original and revised BEB is due to a former overestimation over 10% of the higher ionisation thresholds which can be seen on the bottom graph of figure 3.

Of the first ionic levels, only the \tilde{C} state seems to predissociate. The inner $3\sigma_g$ and $2\sigma_u$ orbitals lie very close in energy and are mixtures of $O(2s)+C(2s)$ and $O(2s)+C(2p_z)$ respectively [1, p.146:table 5]. Ionisation from these inner orbitals seem to lead predominantly to a $C^{++} + 2O$ dissociation [7, p.255]. Removal of a $4\sigma_g$ leads to the \tilde{C} state which predominantly predissociates into $O^+(^4S) + CO(^1\Sigma)$, while higher vibrational states may predissociate into $CO^+(^2\Sigma^+) + O(^3P)$ to a ratio of $CO^+:O^+$ about 1:3 [7, p.253–4].

H₂O. Water is the simplest molecule presented here having the C_{2v} symmetry. The nomenclature of molecular states and orbitals applying to this symmetry can be revised in Hertel and Schulz [31, §4.3.3:p.257–9:table 4.2–3]. Because of its complex vibrational spectrum, ionisation of water from each orbital comprises a rich vibrational band of closely spaced narrow peaks [44, p.4746:fig.1]. Dissociation of the H_2O^+ ion starts after removal of a ($1b_2$) O–H bonding electron. The elastic cross sections relative to H_2O^+ are about $\lesssim 0.5$ for $OH^+:H_2O^+$ and ~ 0.12 for $H^+:H_2O^+$ [7, p.244]. Removal of a ($2a_1$) electron causes complete dissociation with a $H^+:O^+$ ratio of 3:1 [84]. Finally, ejection of a ($1a_1$) electron entails a rapid Auger decay and a subsequent Coulombic explosion leading plausibly to $2H^+ + O^+$ [7, p.246].

NO₂. The orbital symmetries associated to ionisation channels of NO_2 in table 1 are following Baltzer et al. [5, p.451]. There are differences with the notation in [46, table II] and also in the ordering of energy levels. The notable difference in the total ionisation cross section between original and revised BEB in figure 4 is mainly due to the ionisation channels associated with $5a_1$, $1b_1$ and $3b_2$ orbitals whose Hartree-Fock energies are actually about 18% above the experimental ones, supplemented with a 10% overestimation of other thresholds. Despite this inadequacy of binding energies, the agreement of the original BEB with the total ionisation cross section is mesmerising. We believe this agreement to be coincidental.

Like NO, nitric dioxide has a lone electron in its outermost valence shell ($6a_1$). Removing this lone electron makes NO_2^+ linear and isoelectronic with CO_2 . This consequential change of geometry spurs a very dense and rich vibrational spectrum whose adiabatic ionisation threshold may be as low as 9.6 eV [14]. Nevertheless, the onset of ionisation may be considered to start at the vibrational peak centroid around 11.2 eV [5, fig. 5]. Ionisation from all orbitals below the highest occupied molecular

orbital can generate either triplet or singlet states. Nonetheless, this splitting from holes in orbitals deeper than $4b_2$ and $1a_2$ is not visible on photoelectron spectra [5, p.454:fig. 1] and thus we group the split states together. Although most principal higher ionisation states still comply with the one-electron-hole picture, multiconfiguration calculations indicate that some states, such as $(1b_1)^{-1}d^3B_1$ result from significant configuration interaction [11, p.584:table 1]. The binding energies in inner valence orbitals are taken as broad peak positions in the photoelectron spectrum of Baltzer et al. [5, p.455:table 2].

The low dissociation threshold (≈ 2.78 eV) of NO_2 causes all excited ionised states to have high dissociation branching ratios mainly fragmenting into $\text{NO}^+ + \text{O}$ [77, p.687:§IV]. The relative production of NO^+ peaks at about 20 eV to 75 % [4, fig. 5] and slowly seems to stabilises roughly at 50 % at higher energies [62, p.37:fig. 5]. However, state-specific branching ratios are found to vary significantly [22, p.146–7]. The main production of O^+ ions seems to come from the $(3b_2)^{-1}$ state [22, p.146:§3.7]. Here, we have to note that, although predissociation branching ratios may be equally applied to ionic species formed either by photoionisation or electron impact, it is not guaranteed that this analogy of clastic ratios applies equally well for ionisation channels leading to direct dissociation.

O_3 . Ozone is the most complex molecule presently introduced and the only one whose ground state may not be accurately described by a single Hartree-Fock configuration. It involves mixing of the [...] $(1a_2)^2(4b_2)^2(6a_1)^2(2b_1)^0$ and [...] $(1a_2)^0(4b_2)^2(6a_1)^2(2b_1)^2$ configurations [92, §1]. As a result, all the ionisation processes reported in table 1 for O_3 (except for the core $1s$ orbitals) may not be interpreted as a simple hole in an orbital but result from more complex configuration interactions (thus the dashed arrows). Nevertheless, for consistency, we wrote the leading configuration as reported by [92, table 3] for the three first ionic states. The production of O_2^+ has an onset at 13.2 eV, which coincides with the $(1a_2)^{-1}\tilde{B}^2A_2$ state [63, fig. 2:inset] who is thought to predissociate. All higher ionic states dissociate predominantly into $\text{O}_2^+ + \text{O}$. States above the \tilde{B}^2A_2 , involving excitations from the deeper $5a_1$, $1b_1$ and $3b_2$ orbitals, have non-leading mixed configurations and their vibrational bands overlap so that their contributions can be lumped together. In table 1, we selected the vertical energies of the bands (5), (6) and (7,8,9 grouped together), as reported by Couto et al. [15, table I]. However, the assignment of the ionic symmetries is poorly documented and the references attributed do not actually discuss these bands. Thus, we put the labelling into squared brackets. The region above 26 eV in the photoionisation of ozone is even more obscure, as we could not find any information involving the $(3a_1)$ $(2b_2)$ and $(4a_1)$ inner orbitals. For completion, we took the theoretical values reported in Kim et al. [46, table II]. Despite the many uncertainties about modelling partial electron impact ionisation from ozone, the particularly poor agreement of total electron impact ionisation cross sections seen on the last graph of figure 4 should partly be due to inaccuracy in the experimental data which indeed give an unusually low cross section (compared with other triatomic molecules). This was attributed by Kim et al. [46, §III.I] to an inaccurate

normalisation of experimental data of Newson et al. [64]. Hitherto, as far as we know, this discrepancy has not been resolved.

Ozone challenges the BEB model based on an orbital decomposition of molecules as illustrated on the dotted labels on the bottom graph of figure 1. Since the electron-hole picture collapses in the higher excited O_3^+ states, the attribution of the parameter N becomes also uncertain. This exemplifies the need of a more generalised BEB model which is not based on the occupation number N of orbitals (and ionic state multiplicity) but rather on the intensity of the (differential) dipole oscillator strength integrated over each band region. The ionisation cross section may still be decomposed into several partial ones with different thresholds, but the parameters K , N and the labelling of the cross sections must be reconsidered.

5. Conclusion and outlook

We assessed the applicability of the binary-encounter Bethe model to the evaluation of partial ionisation cross sections from electron impact. We determined that its main limitation comes from its construction as a sum of “orbital” cross sections reflecting the structure of a single-configuration Hartree-Fock model, which overall gives a poor description of many of the molecules considered. This limitation is manifest when comparing the theoretical partial ionisation thresholds, systematically overestimating the experimental thresholds observed in photoelectron spectroscopy.

We argue that, in order to yield partial cross sections of ionisation channels in equation (9) consistently, all ionisation thresholds should be taken from experimental data using photo-electron spectroscopy. Unfortunately, this forfeits degradation of the overall performance of the BEB for representing total ionisation cross sections of molecular targets. Indeed for all molecules, the original BEB model using theoretically calculated binding energies from the Hartree-Fock model agrees better with experimental data than when using experimentally determined ionisation thresholds.

Notwithstanding, such observation serves to elucidate how fortuitous compensation of errors endorsed the success of the simple BEB model. This was remarked already in the series of the B-spline R-matrix studies [26, 87, 90, 91] for atomic targets. This observation changes previous conclusions about the performance of the BEB model. We wish to clarify the following:

- I. For atomic targets, spin-forbidden ionisations (see barred arrow \rightarrow on table 1) have negligible contribution. This affects the premise about the proportion of metastable states in the experimental data of atomic nitrogen.
- II. Contributions to the total ionisation cross section from all autoionising states are already encompassed by the BEB model because it assumes that all the Bethe sum (of the dipole oscillator strength) is entirely taken by ionisation processes. If one wishes to model autoionisations separately, one needs to consistently subtract the part of the dipole oscillator strength taken by the latter from the BEB model

(which ceases to be BEB and turns into the BEQ model with $Q < 1$). This misunderstanding affected results on atomic carbon and oxygen.

- III. A higher ionisation threshold induces an inversely proportional reduction of the partial cross section, principally affecting the asymptotic tail of the BEB. This explains why many of the molecules (O_2 , NO_2 , CO_2) which are known to have important optically allowed excitations (not leading to ionisation) could be modelled surprisingly well by the BEB even in the asymptotic region. Normally, one would expect to have an overestimation proportional to the part of the Bethe sum which had not be subtracted, as we now currently have.

The overall tendency of the binary-encounter-Bethe model to overestimate total ionisation is actually not unknown and can be corrected with a reduction of the optical oscillator strength encompassed in a parameter Q used in the BEQ model of Kim and Rudd [48]. In the author's thesis [73, §11.5.4], we could accurately fit Q to reproduce the total ionisation cross sections of atmospheric gases. Yet, we had not used the partial ionisation thresholds as identified here. In this paper, we wish warn readers against fortuitous successes of simple semi-empirical models. Only after using the experimental I will fitting Q open a promising avenue for representing partial cross sections with the binary-encounter-Bethe model. With these issues in mind, we propose that:

- (i) The theoretical binding orbital energies B be replaced by vertical ionisation thresholds I identified in photoelectron spectroscopy as the energy at the maximum of sharp peaks or broad band centroids.
- (ii) The overestimation of the BEB model in the asymptotic region of the total ionisation cross section can now serve to identify the scaling due to the Bethe sum (of the optical oscillator strength) accounted by the more accurate BEQ model.
- (iii) The value of the Bethe scaling parameter K should depend on the process considered and may, but need not, be related to the orbital binding B and kinetic U energies as used in the Burgess denominator given in eq. 2. Indeed, Hwang et al. [36, p.2966] encouraged users to treat U (hence K) as an adjustable parameter. For instance, partial ionisation from the 1s shell (in figure 2) are better modelled with the formula eq. 3 from Guerra et al. [28, eq.(1)]. Furthermore, the K parameter can be adjusted so as to match the BEQ model to the experimental data in the peak region around 100 eV.

Finally, since there are no direct measurements of partial ionisation cross sections for electron impact ionisation, the further application of the BEB model for modelling partial ionisation processes will have to rely on three main sources of indirect comparisons:

- 1) Total ionisation cross sections: further improvement will require including information about the differential dipole oscillator strengths integrated over band regions in the photoelectron spectrum for each transition considered, and therefrom using the BEQ model instead of the BEB (as in Schmalzried [73, §11.5.4]).

- 2) Partial ionisation cross sections: use predictions published from sophisticated *ab initio* models such as the B-spline R-matrix [94] to assess the BEQ partial cross sections.
- 3) Clastic ionisation cross sections: construct models or an average value of branching ratios [34] for processes subsequent to direct ionisation (predissociation, autoionisation and radiative deexcitation) of molecular targets (production of ionic fragments).

Acknowledgements

The authors are grateful to the reviewers for their useful review and suggestions on how to improve the focus of the present article. We benefited from four different reviewers and we believe that their critique has led us to a very fruitful investigation. We acknowledge funding from the State Agency for Research of the Spanish MCIU through the “Center of Excellence Severo Ochoa” award for the Instituto de Astrofísica de Andalucía (SEV-2023-0709), and the Research Council of Norway under contracts 208028/F50, 216872/F50 and 223252/F50 (CoE). N. Lehtinen was supported by the Research Council of Norway under contract 335162/L40.

All the data gathered in this research are freely available through the [elmolcs](#) Python package hosted on Codeberg and now also on PyPI. The python file ([BEB.py](#)) used to produce all our graphs and our table is provided as a supplementary material.

Table 1: Input parameters to the BEB model in eq. 1. Binding electron energies in orbitals identified as partial ionisation thresholds (I), kinetic scaling energies (K) and orbital occupation number or participation to the partial ionisation (N). Processes marked with a barred arrow ($\bar{\rightarrow}$) are optically spin-forbidden (require electron exchange). Dashed arrows ($--\rightarrow$) symbolise that the final state may not be seen as a hole in a subshell but is rather a mixture. Arrows with question marks ($\overset{?}{\rightarrow}$) mean that the process has various subsequent branching ratios. Asterisks (*) mark the presence of predissociation. The last column gives the references for the processes identified and numbers taken. The nomenclature of molecular orbitals can be read in Hertel and Schulz [31, §4.3:p.253–259]

Subshell or Reaction	I (eV)	K (eV)	N	Reference
$(1s)^{-1} \overset{?}{\rightarrow} C^{++} + e^{-}$	296.24	160	2	[9, table. IV:line 26]
$(2s)^{-1} \rightarrow C^{+2} P$	24.98	66.9	2/3	[52]

$(2s)^{-1} \rightarrow C^{+2} S$	23.22	65.1	–	
$(2s)^{-1} \rightarrow C^{+2} D$	20.55	62.5	–	
$(2s)^{-1} \rightarrow C^{+4} P$	16.59	58.5	4/3	
$(2p)^{-1} \rightarrow C^{+2} P$	11.26	45.4	2	
<hr/>				
$(1s)^{-1} \xrightarrow{?} N^{++} + e^{-}$	409.64	223	2	[71]
$(2s)^{-1} \rightarrow N^{+1} P^o$	35.22	100.9	–	[52]
$(2s)^{-1} \rightarrow N^{+3} S^o$	33.78	99.4	3/4	
$(2s)^{-1} \rightarrow N^{+1} D^o$	31.42	97.1	–	
$(2s)^{-1} \rightarrow N^{+3} P^o$	28.08	93.7	–	
$(2s)^{-1} \rightarrow N^{+3} D^o$	25.97	91.6	–	
$(2s)^{-1} \rightarrow N^{+5} S^o$	20.34	86.0	5/4	
$(2p)^{-1} \rightarrow N^{+1} S$	18.59	69.6	–	
$(2p)^{-1} \rightarrow N^{+1} D$	16.43	67.5	–	
$(2p)^{-1} \rightarrow N^{+3} P$	14.55	65.6	3	
<hr/>				
$(1s)^{-1} \xrightarrow{?} O^{++} + e^{-}$	544.54	297	2	[24, 27, §4.1]
$(2s)^{-1} \rightarrow O^{+2} P$	39.98	124.7	2/3	[52]
$(2s)^{-1} \rightarrow O^{+2} S$	37.88	122.6	–	
$(2s)^{-1} \rightarrow O^{+2} D$	34.20	119.0	–	
$(2s)^{-1} \rightarrow O^{+4} P$	28.50	113.3	4/3	
$(2p)^{-1} \rightarrow O^{+2} P^o$	18.64	87.1	6/5	
$(2p)^{-1} \rightarrow O^{+2} D^o$	16.94	85.4	2	
$(2p)^{-1} \rightarrow O^{+4} S^o$	13.62	82.8	4/5	
<hr/>				
$(1s)^{-1} \xrightarrow{?} F^{++} + e^{-}$	696.7	381.3	2	[43, p.466]
$(2s)^{-1} \rightarrow F^{+1} P^o$	47.12	158.6	0.5	[52]
$(2s)^{-1} \rightarrow F^{+3} P^o$	37.89	149.4	1.5	
$(2p)^{-1} \rightarrow F^{+1} S$	22.99	113.9	1/3	
$(2p)^{-1} \rightarrow F^{+1} D$	20.01	110.9	5/3	
$(2p)^{-1} \rightarrow F^{+3} P$	17.42	108.3	3	
<hr/>				
$(1\sigma)^{-1} \xrightarrow{?} C^{++}, O^{++}, C^{+} + O^{+}$	542.57	297	2	[33, p.170]
$(2\sigma)^{-1} \xrightarrow{?} C^{++}, O^{++}, C^{+} + O^{+}$	296.24	160	2	
$(3\sigma)^{-1} \xrightarrow{?} C^{+} + O$	38.9	120.4	2	
$(4\sigma)^{-1} \rightarrow CO^{+} B^2\Sigma^{+}$	19.7	92.9	2	
$(1\pi)^{-1} \rightarrow CO^{+} A^2\Pi$	16.58	70.9	4	
$(5\sigma)^{-1} \rightarrow CO^{+} X^2\Sigma^{+}$	14.01	56.3	2	
<hr/>				
$(1\sigma)^{-1} \xrightarrow{?} N_2^{++}, N^{+} + N^{+}$	409.5	223	4	[33, p.426]
$(2\sigma_g)^{-1} \rightarrow N + N^{+}$	37.8	108.9	2	
$(2\sigma_u)^{-1} \dashrightarrow N_2^{+} C^2\Sigma_u^{+} *$	23.6	86.8	1	
$(2\sigma_u)^{-1} \dashrightarrow N_2^{+} B^2\Sigma_u^{+}$	18.75	81.9	1	
$(1\pi_u)^{-1} \rightarrow N_2^{+} A^2\Pi_u$	16.72	61.0	4	

$(3\sigma_g)^{-1} \rightarrow N_2^+ X^2\Sigma_g^+$	15.58	70.5	2	
$(1\sigma)^{-1} \xrightarrow{?} N^+ + O^+, N^{++}, O^{++}$	543.2	297	2	[33, p.482]
$(2\sigma)^{-1} \xrightarrow{?} N^+ + O^+, N^{++}, O^{++}$	410.2	223	2	
$(3\sigma)^{-1} \xrightarrow{?} N^+ + O$	40.56	117.1	2	
$(4\sigma)^{-1} \dashrightarrow NO^+ c^3\Pi, B^1\Pi^*$	21.72	98.8	2	[21]
$(5\sigma)^{-1} \rightarrow NO^+ A^1\Pi$	18.37	80.6	0.5	
$(5\sigma)^{-1} \rightarrow NO^+ b^3\Pi$	16.6	78.9	1.5	
$(1\pi)^{-1} \xrightarrow{?} NO^+ B'^1\Sigma^+$	22.73	78.1	1/3	
$(1\pi)^{-1} \rightarrow NO^+ W^1\Delta$	18.12	73.5	1/3	
$(1\pi)^{-1} \rightarrow NO^+ A'^1\Sigma^+$	17.88	73.3	1/3	
$(1\pi)^{-1} \rightarrow NO^+ b'^3\Sigma^-$	17.65	73.0	1	
$(1\pi)^{-1} \rightarrow NO^+ w^3\Delta$	16.93	72.3	1	
$(1\pi)^{-1} \rightarrow NO^+ a^3\Sigma^+$	15.73	71.1	1	
$(2\pi)^{-1} \rightarrow NO^+ X^1\Sigma^+$	9.26	74.5	1	
$(1\sigma)^{-1} \xrightarrow{?} O_2^+, O_2^{++}, O + O^+$	543.1	297	4	[33, p.504]
$(2\sigma_g)^{-1} \xrightarrow{?} O_2^+, O + O^+$	39.57	79.73	2	
$(2\sigma_u)^{-1} \rightarrow O_2^+ c^4\Sigma_u^- *$	24.58	90.92	2	[7, p.222–5]
$(3\sigma_g)^{-1} \rightarrow O_2^+ B^2\Sigma_g^- *$	20.3	71.84	2/3	[20]
$(3\sigma_g)^{-1} \rightarrow O_2^+ b^4\Sigma_g^- *$	18.17	71.84	4/3	
$(1\pi_u)^{-1} \rightarrow O_2^+ A^2\Pi_u$	17.15	59.89	4/3	
$(1\pi_u)^{-1} \rightarrow O_2^+ a^4\Pi_u$	16.16	59.89	8/3	
$(1\pi_g)^{-1} \rightarrow O_2^+ X^2\Pi_g$	12.07	84.88	2	
$(1\sigma)^{-1} \xrightarrow{?} C^+2 + O^+$	541.1	297	4	[1, tab.6:p.147]
$(2\sigma_g)^{-1} \xrightarrow{?} C^+2 + O^+$	297.5	160	2	
$(2\sigma_u)^{-1} \xrightarrow{?} C^+ + 2O$	39.7	115.4	2	[3]
$(3\sigma_g)^{-1} \xrightarrow{?} C^+ + 2O$	37.5	115.9	2	
$(4\sigma_g)^{-1} \rightarrow CO_2^+ \tilde{C}^2\Sigma_g^+ *$	19.4	94.7	2	
$(3\sigma_u)^{-1} \rightarrow CO_2^+ \tilde{B}^2\Sigma_u^+ *$	18.1	89.7	2	
$(1\pi_u)^{-1} \rightarrow CO_2^+ \tilde{A}^2\Pi_u$	17.6	67.6	4	
$(1\pi_g)^{-1} \rightarrow CO_2^+ X^2\Pi_g$	13.8	78.2	4	
$(1a_1)^{-1} \xrightarrow{?} 2H^+ + O^+$	539.70	297	2	[79, p.84:table 5.3.1]
$(2a_1)^{-1} \xrightarrow{?} H^+ + H + O$	32.20	102.9	2	
$(1b_2)^{-1} \rightarrow H_2O^+ ^2B_2$	18.51	66.87	2	[7, p.241:table 5]
$(3a_1)^{-1} \rightarrow H_2O^+ ^2A_1$	14.74	74.27	2	
$(1b_1)^{-1} \rightarrow H_2O^+ ^2B_1$	12.62	74.52	2	
$(1a_1)^{-1} \xrightarrow{?} N + 2O^+$	541.3	297	4	[79, p.126:table 5.4.4]
$(2a_1)^{-1} \xrightarrow{?} N^+ + O^+ + O$	412.4	223	2	[79, p.123:table 5.4.3]
$(3a_1)^{-1} \xrightarrow{?} NO^+ + O$	38.9	112	2	[5, table 2]

$(2b_2)^{-1} \xrightarrow{?} \text{NO}^+ + \text{O}$	32.0	110	2	
$(4a_1)^{-1} \xrightarrow{?} \text{NO}^+ + \text{O}$	21.3	100	2	
$(3b_2)^{-1} \xrightarrow{?} \text{NO} + \text{O}^+$	19.06	75.8	2	
$(1b_1)^{-1} \dashrightarrow \text{NO}_2^+ \text{d } ^3\text{B}_1^*$	17.63	90.9	2	
$(5a_1)^{-1} \rightarrow \text{NO}_2^+ \text{c } ^3\text{A}_1^*$	17.45	69	2	
$(4b_2)^{-1} \rightarrow \text{NO}_2^+ \text{B } ^1\text{B}_2^*$	14.60	83.7	0.5	
$(1a_2)^{-1} \rightarrow \text{NO}_2^+ \text{A } ^1\text{A}_2^*$	14.13	83.2	0.5	
$(1a_2)^{-1} \rightarrow \text{NO}_2^+ \text{b } ^3\text{A}_2^*$	13.69	78.9	1.5	
$(4b_2)^{-1} \rightarrow \text{NO}_2^+ \text{a } ^3\text{B}_2^*$	13.06	78.3	1.5	
$(6a_1)^{-1} \rightarrow \text{NO}_2^+ \text{X } ^1\Sigma_g^+$	11.2	87.4	1	
<hr/>				
$(1a_1)^{-1} \xrightarrow{?} 2\text{O}^+ + \text{O}$	546.20	297	2	[6]
$(2a_1)^{-1}, (1b_2)^{-1} \xrightarrow{?} 2\text{O}^+ + \text{O}$	541.50	297	4	
$[(3a_1)^{-1}] \dashrightarrow \text{O}_2^+ + \text{O}$	50.16	128.37	2	[46, table II]
$[(2b_2)^{-1}] \dashrightarrow \text{O}_2^+ + \text{O}$	40.63	121.25	2	
$[(4a_1)^{-1}] \dashrightarrow \text{O}_2^+ + \text{O}$	29.11	118.45	2	
$[\text{O}_3^+ \text{6 } ^2\text{B}_2, \text{5 } ^2\text{B}_1, \dots]^*$	20.00	89.13	[2]	[15, table I]
$[\text{O}_3^+ \text{3 } ^2\text{A}_1, \text{4 } ^2\text{B}_2]^*$	17.30	75.85	[2]	
$[\text{O}_3^+ \text{2 } ^2\text{B}_1]^*$	16.57	93.66	[2]	
$(1a_2)^{-1} \dashrightarrow \text{O}_3^+ \tilde{\text{B}}^2\text{A}_2^*$	13.54	87.36	2	
$(4b_2)^{-1} \dashrightarrow \text{O}_3^+ \tilde{\text{A}}^2\text{B}_2$	13.00	89.56	2	
$(6a_1)^{-1} \dashrightarrow \text{O}_3^+ \tilde{\text{X}}^2\text{A}_1$	12.73	77.85	2	

References

- [1] C.J. Allan, U. Gelius, D.A. Allison, G. Johansson, H. Siegbahn, and K. Siegbahn. ESCA studies of CO₂, CS₂ and COS. *J. Electron Spectrosc. Relat. Phenom.*, 1(2):131–151, 1972. ISSN 0368-2048. doi: [https://doi.org/10.1016/0368-2048\(72\)80027-6](https://doi.org/10.1016/0368-2048(72)80027-6). URL <https://www.sciencedirect.com/science/article/pii/0368204872800276>.
- [2] D P Almeida, A C Fontes, and C F L Godinho. Electron-impact ionization cross section of neon (σ_{n+} , $n=1-5$). *J. Phys. B: At. Mol. Opt. Phys.*, 28(15): 3335, aug 1995. doi: 10.1088/0953-4075/28/15/022. URL <https://dx.doi.org/10.1088/0953-4075/28/15/022>.
- [3] Michele Aresta, Angela Dibenedetto, and Eugenio Quaranta. *The Carbon Dioxide Molecule*, pages 1–34. Springer Berlin Heidelberg, Berlin, Heidelberg, 2016. ISBN 978-3-662-46831-9. doi: 10.1007/978-3-662-46831-9_1. URL https://doi.org/10.1007/978-3-662-46831-9_1.
- [4] Jennifer W. Au and C. E. Brion. Absolute oscillator strenghts for the valence-shell photoabsorption (2–200 eV) and the molecular and dissociative photoionization

- (11–80 eV) of nitrogen dioxide. *Chem. Phys.*, 218(1):109–126, 1997. ISSN 0301-0104. doi: [https://doi.org/10.1016/S0301-0104\(97\)00065-7](https://doi.org/10.1016/S0301-0104(97)00065-7). URL <https://www.sciencedirect.com/science/article/pii/S0301010497000657>.
- [5] P. Baltzer, L. Karlsson, B. Wannberg, D.M.P. Holland, M.A. MacDonald, M.A. Hayes, and J.H.D. Eland. An experimental study of the valence shell photoelectron spectrum of the NO₂ molecule. *Chem. Phys.*, 237(3):451–470, 1998. ISSN 0301-0104. doi: [https://doi.org/10.1016/S0301-0104\(98\)00240-7](https://doi.org/10.1016/S0301-0104(98)00240-7). URL <https://www.sciencedirect.com/science/article/pii/S0301010498002407>.
- [6] M.Salim Banna, David C. Frost, Charles A. McDowell, Louis Noodleman, and Barry Wallbank. A study of the core electron binding energies of ozone by x-ray photoelectron spectroscopy and the X α scattered wave method. *Chem. Phys. Lett.*, 49(2):213–217, 1977. ISSN 0009-2614. doi: [https://doi.org/10.1016/0009-2614\(77\)80572-1](https://doi.org/10.1016/0009-2614(77)80572-1). URL <https://www.sciencedirect.com/science/article/pii/0009261477805721>.
- [7] Joseph Berkowitz. Chapter VI - partial cross sections. In Joseph Berkowitz, editor, *Photoabsorption, Photoionization, and Photoelectron Spectroscopy*, pages 155–357. Academic Press, 1979. ISBN 978-0-12-091650-4. doi: <https://doi.org/10.1016/B978-0-12-091650-4.50012-8>. URL <https://www.sciencedirect.com/science/article/pii/B9780120916504500128>.
- [8] E Brook, M F A Harrison, and A C H Smith. Measurements of the electron impact ionisation cross sections of He, C, O and N atoms. *J. Phys. B: At. Mol. Phys.*, 11(17):3115–3132, September 1978. doi: 10.1088/0022-3700/11/17/021. URL <https://doi.org/10.1088/0022-3700/11/17/021>.
- [9] Reinhard Bruch, Kwong T. Chung, William L. Luken, and John C. Culberson. Recalibration of the KLL Auger spectrum of carbon. *Phys. Rev. A*, 31:310–315, Jan 1985. doi: 10.1103/PhysRevA.31.310. URL <https://link.aps.org/doi/10.1103/PhysRevA.31.310>.
- [10] Paul E. Cade, K. D. Sales, and Arnold C. Wahl. Electronic structure of diatomic molecules. III. A. Hartree—Fock wavefunctions and energy quantities for N₂(X¹ Σ_g^+) and N₂⁺(X² Σ_g^+ , A² Π_u , B² Σ_u^+) molecular ions. *J. Chem. Phys.*, 44(5):1973–2003, 03 1966. ISSN 0021-9606. doi: 10.1063/1.1726972. URL <https://doi.org/10.1063/1.1726972>.
- [11] Hai-Bo Chang and Ming-Bao Huang. A theoretical study on the electronic states and O-loss photodissociation of the NO₂⁺ ion. *ChemPhysChem*, 10(3):582–589, 2009. doi: <https://doi.org/10.1002/cphc.200800626>. URL <https://chemistry-europe.onlinelibrary.wiley.com/doi/abs/10.1002/cphc.200800626>.
- [12] O. Chanrion and T. Neubert. Production of runaway electrons by negative streamer discharges. *J. Geophys. Res. : Space Phys.*, 115(A00E32), 2010. doi: 10.1029/2009JA014774. URL <https://agupubs.onlinelibrary.wiley.com/doi/abs/10.1029/2009JA014774>.

- [13] E. Clementi and D. L. Raimondi. Atomic Screening Constants from SCF Functions. *J. Chem. Phys.*, 38(11):2686–2689, 06 1963. ISSN 0021-9606. doi: 10.1063/1.1733573. URL <https://doi.org/10.1063/1.1733573>.
- [14] D. E. Clemmer and P. B. Armentrout. Direct determination of the adiabatic ionization energy of NO₂ as measured by guided ion-beam mass spectrometry. *J. Chem. Phys.*, 97(4):2451–2458, 08 1992. ISSN 0021-9606. doi: 10.1063/1.463083. URL <https://doi.org/10.1063/1.463083>.
- [15] H. Couto, A. Mocellin, C. D. Moreira, M. P. Gomes, A. Naves de Brito, and M. C. A. Lopes. Threshold photoelectron spectroscopy of ozone. *J. Chem. Phys.*, 124(20):204311, 05 2006. ISSN 0021-9606. doi: 10.1063/1.2200702. URL <https://doi.org/10.1063/1.2200702>.
- [16] Sébastien Célestin and Victor P. Pasko. Energy and fluxes of thermal runaway electrons produced by exponential growth of streamers during the stepping of lightning leaders and in transient luminous events. *J. Geophys. Res. : Space Phys.*, 116(A3), 2011. doi: 10.1029/2010JA016260. URL <https://agupubs.onlinelibrary.wiley.com/doi/abs/10.1029/2010JA016260>.
- [17] H. Deutsch, P. Scheier, K. Becker, and T. D. Märk. Revised high energy behavior of the Deutsch-Märk (DM) formula for the calculation of electron impact ionization cross sections of atoms. *Int J Mass Spectrom*, 233(1):13–17, 2004. ISSN 1387-3806. doi: <https://doi.org/10.1016/j.ijms.2003.06.002>. URL <https://www.sciencedirect.com/science/article/pii/S1387380603004962>. Special Issue: In honour of Tilmann Märk.
- [18] N.Lj. Djurić, I.M. Čadež, and M.V. Kurepa. H₂O and D₂O total ionization cross-sections by electron impact. *Int. J. Mass Spectrom.*, 83(3):R7–R10, 1988. ISSN 0168-1176. doi: [https://doi.org/10.1016/0168-1176\(88\)80038-7](https://doi.org/10.1016/0168-1176(88)80038-7). URL <https://www.sciencedirect.com/science/article/pii/0168117688800387>.
- [19] Brian J. Duke and Brian O’Leary. Non-Koopmans’ Molecules. *J. Chem. Educ.*, 72(6):501, June 1995. ISSN 0021-9584. doi: 10.1021/ed072p501. URL <https://doi.org/10.1021/ed072p501>.
- [20] O. Edqvist, E. Lindholm, L. E. Selin, and L. Åsbrink. On the photoelectron spectrum of O₂. *Phys Scripta*, 1(1):25–30, January 1970. doi: 10.1088/0031-8949/1/1/004. URL <https://doi.org/10.1088/0031-8949/1/1/004>.
- [21] O. Edqvist, L. Åsbrink, and E. Lindholm. On the photoelectron spectrum of NO. *Zeitschrift für Naturforschung A*, 26(9):1407–1410, 1971. doi: doi:10.1515/zna-1971-0906. URL <https://doi.org/10.1515/zna-1971-0906>.
- [22] J.H.D. Eland and L. Karlsson. Dissociative photoionisation of NO₂ up to 26 eV. *Chem. Phys.*, 237(1):139–148, 1998. ISSN 0301-0104. doi: [https://doi.org/10.1016/S0301-0104\(98\)00237-7](https://doi.org/10.1016/S0301-0104(98)00237-7). URL <https://www.sciencedirect.com/science/article/pii/S0301010498002377>.
- [23] Peter Erman. Direct measurement of the N₂⁺ C state predissociation probability.

- Phys Scr*, 14(1-2):51, July 1976. doi: 10.1088/0031-8949/14/1-2/010. URL <https://dx.doi.org/10.1088/0031-8949/14/1-2/010>.
- [24] Federica Frati, Myrtille O. J. Y. Hunault, and Frank M. F. de Groot. Oxygen K-edge X-ray absorption spectra. *Chem. Rev.*, 120(9):4056–4110, 2020. doi: 10.1021/acs.chemrev.9b00439. URL <https://doi.org/10.1021/acs.chemrev.9b00439>. PMID: 32275144.
- [25] Gaudin, Albert and Hagemann, Robert. Déterminations absolues des sections efficaces totales et partielles d’ionisation de l’hélium, du néon, de l’argon et de l’acétylène, pour des électrons de 100 à 2000 eV. *J. Chim. Phys.*, 64:1209–1221, 1967. doi: 10.1051/jcp/1967641209. URL <https://doi.org/10.1051/jcp/1967641209>.
- [26] Viktor Gedeon, Sergej Gedeon, Vladimir Lazur, Elizabeth Nagy, Oleg Zatsarinny, and Klaus Bartschat. *b*-spline *r*-matrix-with-pseudostates calculations for electron-impact excitation and ionization of fluorine. *Phys. Rev. A*, 89:052713, May 2014. doi: 10.1103/PhysRevA.89.052713. URL <https://link.aps.org/doi/10.1103/PhysRevA.89.052713>.
- [27] T. W. Gorczyca, M. A. Bautista, M. F. Hasoglu, J. García, E. Gatuuzz, J. S. Kaastra, T. R. Kallman, S. T. Manson, C. Mendoza, A. J. J. Raassen, C. P. de Vries, and O. Zatsarinny. A comprehensive X-ray absorption model for atomic oxygen. *ApJ*, 779(1):78, nov 2013. doi: 10.1088/0004-637X/779/1/78. URL <https://dx.doi.org/10.1088/0004-637X/779/1/78>.
- [28] M. Guerra, F. Parente, P. Indelicato, and J. P. Santos. Modified binary encounter Bethe model for electron-impact ionization. *Int J Mass Spectrom*, 313:1–7, 2012. ISSN 1387-3806. doi: <https://doi.org/10.1016/j.ijms.2011.12.003>. URL <https://www.sciencedirect.com/science/article/pii/S138738061100474X>.
- [29] G. J. M. Hagelaar and L. C. Pitchford. Solving the boltzmann equation to obtain electron transport coefficients and rate coefficients for fluid models. *Plasma Sources Sci. Technol.*, 14(4):722, October 2005. doi: 10.1088/0963-0252/14/4/011. URL <https://dx.doi.org/10.1088/0963-0252/14/4/011>.
- [30] Todd R. Hayes, Robert C. Wetzel, and Robert S. Freund. Absolute electron-impact-ionization cross-section measurements of the halogen atoms. *Phys. Rev. A*, 35:578–584, Jan 1987. doi: 10.1103/PhysRevA.35.578. URL <https://link.aps.org/doi/10.1103/PhysRevA.35.578>.
- [31] Ingolf V. Hertel and Claus-Peter Schulz. *Atoms, Molecules and Optical Physics 2: Molecules and Photons - Spectroscopy and Collisions*. Springer Berlin Heidelberg, Berlin, Heidelberg, 2015. ISBN 978-3-642-54313-5. doi: 10.1007/978-3-642-54313-5. URL <https://doi.org/10.1007/978-3-642-54313-5>.
- [32] K. P. Huber. The excited electronic states of the NO⁺ ion. *Can J Phys*, 46(15):1691–1695, 1968. doi: 10.1139/p68-501. URL <https://doi.org/10.1139/p68-501>.

- [33] K. P. Huber and G. Herzberg. *IV. Constants of Diatomic Molecules*. Molecular Spectra and Molecular Structure. Springer US, Boston, MA, 1979. ISBN 978-1-4757-0961-2. doi: 10.1007/978-1-4757-0961-2_2. URL https://doi.org/10.1007/978-1-4757-0961-2_2.
- [34] Stefan E. Huber, Andreas Mauracher, Daniel Süß, Ivan Sukuba, Jan Urban, Dmitry Borodin, and Michael Probst. Total and partial electron impact ionization cross sections of fusion-relevant diatomic molecules. *J. Chem. Phys.*, 150(2):024306, 2019. doi: 10.1063/1.5063767. URL <https://doi.org/10.1063/1.5063767>.
- [35] W. M. Huo and Y.-K. Kim. Electron collision cross-section data for plasma modeling. *IEEE Trans. Plasma Sci.*, 27(5):1225–1240, 1999. doi: 10.1109/27.799798.
- [36] W. Hwang, Y.-K. Kim, and M. E. Rudd. New model for electron-impact ionization cross sections of molecules. *J. Chem. Phys.*, 104(8):2956–2966, 1996. doi: 10.1063/1.471116. URL <https://doi.org/10.1063/1.471116>.
- [37] Philipp Hönicke, Rainer Unterumsberger, Nils Wauschkuhn, Markus Krämer, Burkhard Beckhoff, Paul Indelicato, Jorge Sampaio, José Pires Marques, Mauro Guerra, Fernando Parente, and José Paulo Santos. Experimental and theoretical approaches for determining the K-shell fluorescence yield of carbon. *Radiat. Phys. Chem.*, 202:110501, 2023. ISSN 0969-806X. doi: <https://doi.org/10.1016/j.radphyschem.2022.110501>. URL <https://www.sciencedirect.com/science/article/pii/S0969806X22005370>.
- [38] M. Inokuti, S. J. Buckman, M. T. Elford, and H. Tawara. 2. Electron collisions with atoms. In Y. Itikawa, editor, *Interactions of Photons and Electrons with Atoms*, volume 17 A of *Landolt-Börnstein - Group I Elementary Particles, Nuclei and Atoms*, chapter 2. Springer-Verlag Berlin Heidelberg, 2000. doi: 10.1007/10547143_2. URL https://materials.springer.com/lb/docs/sm_lbs_978-3-540-69716-9_2.
- [39] Mitio Inokuti. Inelastic collisions of fast charged particles with atoms and molecules—The Bethe theory revisited. *Rev. Mod. Phys.*, 43:297–347, July 1971. doi: 10.1103/RevModPhys.43.297. URL <https://link.aps.org/doi/10.1103/RevModPhys.43.297>. In this work, M represents the reduced mass of the system $m_1 m_2 / (m_1 + m_2)$, which is noted μ in our work.
- [40] Yukikazu Itikawa. Cross sections for electron collisions with nitrogen molecules. *J Phys Chem Ref Data*, 35(1):31–53, 2006. doi: 10.1063/1.1937426. URL <https://doi.org/10.1063/1.1937426>.
- [41] Yukikazu Itikawa. Cross sections for electron collisions with oxygen molecules. *J Phys Chem Ref Data*, 38(1):1–20, 2009. doi: 10.1063/1.3025886. URL <https://doi.org/10.1063/1.3025886>.
- [42] Yukikazu Itikawa. Cross sections for electron collisions with nitric oxide. *J Phys Chem Ref Data*, 45(3):033106, 2016. doi: 10.1063/1.4961372. URL <https://doi.org/10.1063/1.4961372>.

- [43] W. L. Jolly, K. D. Bomben, and C. J. Eyermann. Core-electron binding energies for gaseous atoms and molecules. *Atom Data Nucl Data*, 31(3):433–493, 1984. ISSN 0092-640X. doi: [https://doi.org/10.1016/0092-640X\(84\)90011-1](https://doi.org/10.1016/0092-640X(84)90011-1). URL <http://www.sciencedirect.com/science/article/pii/0092640X84900111>.
- [44] L. Karlsson, L. Mattsson, R. Jadrny, R. G. Albridge, S. Pinchas, T. Bergmark, and K. Siegbahn. Isotopic and vibronic coupling effects in the valence electron spectra of H₂ 16O, H₂ 18O, and D₂ 16O. *J. Chem. Phys.*, 62(12):4745–4752, 06 1975. ISSN 0021-9606. doi: 10.1063/1.430423. URL <https://doi.org/10.1063/1.430423>.
- [45] Y. B. Kim, K. Stephan, E. Märk, and T. D. Märk. Single and double ionization of nitric oxide by electron impact from threshold up to 180 eV. *J. Chem. Phys.*, 74(12):6771–6776, 06 1981. ISSN 0021-9606. doi: 10.1063/1.441082. URL <https://doi.org/10.1063/1.441082>.
- [46] Y.-K. Kim, W. Hwang, N. M. Weinberger, M. A. Ali, and M. E. Rudd. Electron-impact ionization cross sections of atmospheric molecules. *J. Chem. Phys.*, 106(3):1026–1033, 01 1997. ISSN 0021-9606. doi: 10.1063/1.473186. URL <https://doi.org/10.1063/1.473186>.
- [47] Yong-Ki Kim and Jean-Paul Desclaux. Ionization of carbon, nitrogen, and oxygen by electron impact. *Phys. Rev. A*, 66:012708, July 2002. doi: 10.1103/PhysRevA.66.012708. URL <https://link.aps.org/doi/10.1103/PhysRevA.66.012708>.
- [48] Yong-Ki Kim and M. Eugene Rudd. Binary-encounter-dipole model for electron-impact ionization. *Phys. Rev. A*, 50:3954–3967, November 1994. doi: 10.1103/PhysRevA.50.3954. URL <https://link.aps.org/doi/10.1103/PhysRevA.50.3954>.
- [49] Yong-Ki Kim, José Paulo Santos, and Fernando Parente. Extension of the binary-encounter-dipole model to relativistic incident electrons. *Phys. Rev. A*, 62:052710, October 2000. doi: 10.1103/PhysRevA.62.052710. URL <https://link.aps.org/doi/10.1103/PhysRevA.62.052710>.
- [50] Toshikatsu Koga, Katsutoshi Kanayama, Shinya Watanabe, and Ajit J. Thakkar. Analytical hartree–fock wave functions subject to cusp and asymptotic constraints: He to Xe, Li⁺ to Cs⁺, H⁻ to I⁻. *Int J Quantum Chem*, 71(6):491–497, 1999. doi: 10.1002/(SICI)1097-461X(1999)71:6<491::AID-QUA6>3.0.CO;2-T. URL [https://doi.org/10.1002/\(SICI\)1097-461X\(1999\)71:6<491::AID-QUA6>3.0.CO;2-T](https://doi.org/10.1002/(SICI)1097-461X(1999)71:6<491::AID-QUA6>3.0.CO;2-T).
- [51] T Koopmans. Über die Zuordnung von Wellenfunktionen und Eigenwerten zu den Einzelnen Elektronen Eines Atoms. *Physica*, 1(1):104–113, 1934. ISSN 0031-8914. doi: [https://doi.org/10.1016/S0031-8914\(34\)90011-2](https://doi.org/10.1016/S0031-8914(34)90011-2). URL <https://www.sciencedirect.com/science/article/pii/S0031891434900112>.
- [52] A. Kramida, Yu. Ralchenko, J. Reader, and NIST ASD Team. NIST Atomic Spectra Database (version 5.9). [Online], 2022. URL <https://physics.nist.gov/asd>. [Sat May 28 2022].
- [53] E. E. Kunhardt and Y. Tzeng. Role of electron-molecule angular scattering in shaping the electron-velocity distribution. *Phys. Rev. A*, 34:2158–2166, September

1986. doi: 10.1103/PhysRevA.34.2158. URL <https://link.aps.org/doi/10.1103/PhysRevA.34.2158>.
- [54] C. Köhn and U. Ebert. The structure of ionization showers in air generated by electrons with 1 MeV energy or less. *Plasma Sources Sci. Technol.*, 23(4):045001, June 2014. doi: 10.1088/0963-0252/23/4/045001. URL <https://doi.org/10.1088%2F0963-0252%2F23%2F4%2F045001>.
- [55] H. Lefebvre-Brion. Intensity anomaly in the photoelectron spectrum of NO. *Chem. Phys. Lett.*, 9(5):463–464, 1971. ISSN 0009-2614. doi: [https://doi.org/10.1016/0009-2614\(71\)80269-5](https://doi.org/10.1016/0009-2614(71)80269-5). URL <https://www.sciencedirect.com/science/article/pii/0009261471802695>.
- [56] B. G. Lindsay and M. A. Mangan. 5.1 Ionization. In Y. Itikawa, editor, *Interactions of Photons and Electrons with Molecules*, volume 17 C of *Landolt-Börnstein - Group I Elementary Particles, Nuclei and Atoms*. Springer-Verlag Berlin Heidelberg, 2003. doi: 10.1007/10874891_2. URL https://materials.springer.com/lb/docs/sm_lbs_978-3-540-45843-2_2.
- [57] B. G. Lindsay, M. A. Mangan, H. C. Straub, and R. F. Stebbings. Absolute partial cross sections for electron-impact ionization of NO and NO₂ from threshold to 1000 eV. *J. Chem. Phys.*, 112(21):9404–9410, 06 2000. ISSN 0021-9606. doi: 10.1063/1.481559. URL <https://doi.org/10.1063/1.481559>.
- [58] Mantian Liu, Zhu An, Changhuan Tang, Zhengming Luo, Xiufeng Peng, and Xianguan Long. Experimental electron-impact K-shell ionization cross sections. *Atom. Data Nucl. Data*, 76(2):213–234, 2000. ISSN 0092-640X. doi: <https://doi.org/10.1006/adnd.2000.0843>. URL <https://www.sciencedirect.com/science/article/pii/S0092640X0090843X>.
- [59] Xavier Llovet, Cedric J. Powell, Francesc Salvat, and Aleksander Jablonski. Cross sections for inner-shell ionization by electron impact. *J Phys Chem Ref Data*, 43(1):013102, 2014. doi: 10.1063/1.4832851. URL <https://doi.org/10.1063/1.4832851>.
- [60] J.C. Lorquet and M. Desouter. Excited states of gaseous ions. Transitions to and predissociation of the C²Σ_u⁺ state of N₂⁺. *Chem Phys Lett*, 16(1):136–140, 1972. ISSN 0009-2614. doi: [https://doi.org/10.1016/0009-2614\(72\)80475-5](https://doi.org/10.1016/0009-2614(72)80475-5). URL <https://www.sciencedirect.com/science/article/pii/0009261472804755>.
- [61] Wolfgang Lotz. An empirical formula for the electron-impact ionization cross-section. *Z. Für Phys.*, 206(2):205–211, 1967. ISSN 0044-3328. doi: 10.1007/BF01325928. URL <https://doi.org/10.1007/BF01325928>.
- [62] Toshio Masuoka and Ataru Kobayashi. Single- and double-photoionization cross-sections of nitrogen dioxide (NO₂) and ionic fragmentation of NO₂⁺ and NO₂²⁺. *Chem. Phys.*, 302(1):31–41, 2004. ISSN 0301-0104. doi: <https://doi.org/10.1016/j.chemphys.2004.03.009>. URL <https://www.sciencedirect.com/science/article/pii/S0301010404001193>.

- [63] A. Mocellin, K. Wiesner, F. Burmeister, O. Björneholm, and A. Naves de Brito. Experimental study of photoionization of ozone in the 12 to 21 eV region. *J. Chem. Phys.*, 115(11):5041–5046, 09 2001. ISSN 0021-9606. doi: 10.1063/1.1394945. URL <https://doi.org/10.1063/1.1394945>.
- [64] Karl A. Newson, Stephanie M. Luc, Stephen D. Price, and Nigel J. Mason. Electron-impact ionization of ozone. *Int. J. Mass Spectrom.*, 148(3):203–213, 1995. ISSN 0168-1176. doi: [https://doi.org/10.1016/0168-1176\(95\)04300-A](https://doi.org/10.1016/0168-1176(95)04300-A). URL <https://www.sciencedirect.com/science/article/pii/016811769504300A>.
- [65] O J Orient and S K Srivastava. Electron impact ionisation of H₂O, CO, CO₂ and CH₄. *J. Phys. B: At. Mol. Phys.*, 20(15):3923, aug 1987. doi: 10.1088/0022-3700/20/15/036. URL <https://dx.doi.org/10.1088/0022-3700/20/15/036>.
- [66] S. T. Perkins, D. E. Cullen, M. H. Chen, J. Rathkopf, J. Scofield, and J. H. Hubbell. Tables and graphs of atomic subshell and relaxation data derived from the LLNL Evaluated Atomic Data Library (EADL), Z = 1–100. Technical report, Lawrence Livermore National Lab. (LLNL), 10 1991. URL <https://www.osti.gov/biblio/10121422>.
- [67] W. C. Price. Photoelectron spectroscopy and molecular structure. *Int. Rev. Phys. Chem.*, 1(1):1–30, 1981. doi: 10.1080/01442358109353240. URL <https://doi.org/10.1080/01442358109353240>.
- [68] Donald Rapp and Paula Englander-Golden. Total cross sections for ionization and attachment in gases by electron impact. I. Positive ionization. *J. Chem. Phys.*, 43(5):1464–1479, 1965. doi: 10.1063/1.1696957. URL <https://doi.org/10.1063/1.1696957>.
- [69] R. Rejoub, B. G. Lindsay, and R. F. Stebbings. Determination of the absolute partial and total cross sections for electron-impact ionization of the rare gases. *Phys. Rev. A*, 65:042713, Apr 2002. doi: 10.1103/PhysRevA.65.042713. URL <https://link.aps.org/doi/10.1103/PhysRevA.65.042713>.
- [70] M. A. Ridenti, L. L. Alves, V. Guerra, and J. Amorim. The role of rotational mechanisms in electron swarm parameters at low reduced electric field in N₂, O₂ and H₂. *Plasma Sources Sci. Technol.*, 24(3):035002, April 2015. doi: 10.1088/0963-0252/24/3/035002. URL <https://doi.org/10.1088/0963-0252/24/3/035002>.
- [71] M. M. Sant’Anna, A. S. Schlachter, G. Öhrwall, W. C. Stolte, D. W. Lindle, and B. M. McLaughlin. K-shell X-ray spectroscopy of atomic nitrogen. *Phys. Rev. Lett.*, 107:033001, Jul 2011. doi: 10.1103/PhysRevLett.107.033001. URL <https://link.aps.org/doi/10.1103/PhysRevLett.107.033001>.
- [72] J. P. Santos, F. Parente, and Y.-K. Kim. Cross sections for K-shell ionization of atoms by electron impact. *J. Phys. B: At. Mol. Opt. Phys.*, 36(21):4211–4224, October 2003. doi: 10.1088/0953-4075/36/21/002. URL <https://doi.org/10.1088/0953-4075/36/21/002>.

- [73] A. Schmalzried. *Electron thermal runaway in atmospheric electrified gases: a microscopic approach*. PhD thesis, Instituto de Astrofísica de Andalucía, 2023. URL <http://hdl.handle.net/10261/338079>.
- [74] B. L. Schram, F. J. De Heer, M. J. van der Wiel, and J. Kistemaker. Ionization cross sections for electrons (0.6–20 keV) in noble and diatomic gases. *Physica*, 31(1):94–112, 1965. ISSN 0031-8914. doi: [https://doi.org/10.1016/0031-8914\(65\)90109-6](https://doi.org/10.1016/0031-8914(65)90109-6). URL <https://www.sciencedirect.com/science/article/pii/0031891465901096>.
- [75] B. L. Schram, H. R. Moustafa, J. Schutten, and F. J. de Heer. Ionization cross sections for electrons (100–600 eV) in noble and diatomic gases. *Physica*, 32(4):734–740, 1966. ISSN 0031-8914. doi: [https://doi.org/10.1016/0031-8914\(66\)90005-X](https://doi.org/10.1016/0031-8914(66)90005-X). URL <https://www.sciencedirect.com/science/article/pii/003189146690005X>.
- [76] Zhenjie Shen, Enliang Wang, Maomao Gong, Xu Shan, and Xiangjun Chen. Electron-impact ionization cross sections for nitrogen molecule from 250 to 8000 eV. *J Electron Spectrosc*, 225:42–48, 2018. ISSN 0368-2048. doi: <https://doi.org/10.1016/j.elspec.2018.03.009>. URL <http://www.sciencedirect.com/science/article/pii/S0368204817302931>.
- [77] Kazuhiko Shibuya, Shinzo Suzuki, Takashi Imamura, and Inosuke Koyano. Dissociation of state-selected NO₂⁺ ions studied by threshold photoelectron-photoion coincidence techniques. *J. Phys. Chem. A*, 101(4):685–689, January 1997. ISSN 1089-5639. doi: 10.1021/jp962031f. URL <https://doi.org/10.1021/jp962031f>.
- [78] I. Shimamura and K. Takayanagi, editors. *Electron-molecule collisions*. Physics of atoms and molecules. Plenum Press, New York [etc.], 1984. ISBN 0-306-41531-3. doi: 10.1007/978-1-4613-2357-0. URL <https://link.springer.com/book/10.1007/978-1-4613-2357-0>.
- [79] K. Siegbahn, C. Nordling, G. Johansson, J. Hedman, P. F. Hedén, K. Hamrin, U. Gelius, T. Bergmark, L. O. Werme, R. Manne, et al. *ESCA: Applied to Free Molecules*. North-Holland Publishing Company, 1969. URL https://books.google.es/books?id=PM_bxQECAAJ.
- [80] Kai Siegbahn, Carl Nordling, and Anders Fahlman. *ESCA : atomic, molecular and solid state structure studied by means of electron spectroscopy*. Almqvist and Wiksell, Uppsala, 1967. URL <http://lib.ugent.be/catalog/rug01:001343982>.
- [81] M. Šimek and Z. Bonaventura. Non-equilibrium kinetics of the ground and excited states in N₂–O₂ under nanosecond discharge conditions: extended scheme and comparison with available experimental observations. *J. Phys. D: Appl. Phys.*, 51(50):504004, October 2018. doi: 10.1088/1361-6463/aadcd1. URL <https://doi.org/10.1088/1361-6463/aadcd1>.
- [82] H. C. Straub, P. Renault, B. G. Lindsay, K. A. Smith, and R. F. Stebbings. Absolute partial cross sections for electron-impact ionization of H₂, N₂, and O₂ from threshold

- to 1000 eV. *Phys. Rev. A*, 54:2146–2153, September 1996. doi: 10.1103/PhysRevA.54.2146. URL <https://link.aps.org/doi/10.1103/PhysRevA.54.2146>.
- [83] H. C. Straub, B. G. Lindsay, K. A. Smith, and R. F. Stebbings. Absolute partial cross sections for electron-impact ionization of H₂O and D₂O from threshold to 1000 eV. *J. Chem. Phys.*, 108(1):109–116, 01 1998. ISSN 0021-9606. doi: 10.1063/1.475367. URL <https://doi.org/10.1063/1.475367>.
- [84] K.H. Tan, C.E. Brion, Ph.E. Van der Leeuw, and M.J. van der Wiel. Absolute oscillator strengths (10–60 eV) for the photoabsorption, photoionisation and fragmentation of H₂O. *Chem. Phys.*, 29(3):299–309, 1978. ISSN 0301-0104. doi: [https://doi.org/10.1016/0301-0104\(78\)85080-0](https://doi.org/10.1016/0301-0104(78)85080-0). URL <https://www.sciencedirect.com/science/article/pii/0301010478850800>.
- [85] H. Tanaka, M. J. Brunger, L. Campbell, H. Kato, M. Hoshino, and A. R. P. Rau. Scaled plane-wave Born cross sections for atoms and molecules. *Rev. Mod. Phys.*, 88:025004, May 2016. doi: 10.1103/RevModPhys.88.025004. URL <https://link.aps.org/doi/10.1103/RevModPhys.88.025004>.
- [86] H. Tawara, K.G. Harrison, and F.J. De Heer. X-ray emission cross sections and fluorescence yields for light atoms and molecules by electron impact. *Physica*, 63(2):351–367, 1973. ISSN 0031-8914. doi: [https://doi.org/10.1016/0031-8914\(73\)90321-2](https://doi.org/10.1016/0031-8914(73)90321-2). URL <https://www.sciencedirect.com/science/article/pii/0031891473903212>.
- [87] S. S. Tayal and Oleg Zatsarinny. *B*-spline *R*-matrix-with-pseudostates approach for excitation and ionization of atomic oxygen by electron collisions. *Phys. Rev. A*, 94:042707, October 2016. doi: 10.1103/PhysRevA.94.042707. URL <https://link.aps.org/doi/10.1103/PhysRevA.94.042707>.
- [88] W R Thompson, M B Shah, and H B Gilbody. Single and double ionization of atomic oxygen by electron impact. *J. Phys. B: At. Mol. Opt. Phys.*, 28(7):1321–1330, April 1995. doi: 10.1088/0953-4075/28/7/023. URL <https://doi.org/10.1088/0953-4075/28/7/023>.
- [89] L Vriens. Electron exchange in binary encounter collision theory. *Proc. Phys. Soc.*, 89(1):13–21, September 1966. doi: 10.1088/0370-1328/89/1/304. URL <https://doi.org/10.1088/0370-1328/89/1/304>.
- [90] Yang Wang, Oleg Zatsarinny, and Klaus Bartschat. *b*-spline *r*-matrix-with-pseudostates calculations for electron-impact excitation and ionization of carbon. *Phys. Rev. A*, 87:012704, Jan 2013. doi: 10.1103/PhysRevA.87.012704. URL <https://link.aps.org/doi/10.1103/PhysRevA.87.012704>.
- [91] Yang Wang, Oleg Zatsarinny, and Klaus Bartschat. *B*-spline *R*-matrix-with-pseudostates calculations for electron-impact excitation and ionization of nitrogen. *Phys. Rev. A*, 89:062714, June 2014. doi: 10.1103/PhysRevA.89.062714. URL <https://link.aps.org/doi/10.1103/PhysRevA.89.062714>.
- [92] K Wiesner, R.F Fink, S.L Sorensen, M Andersson, R Feifel, I Hjelte, C Miron, A Naves de Brito, L Rosenqvist, H Wang, S Svensson, and O Björneholm.

- Valence photoionization and resonant core excitation of ozone – experimental and theoretical study of the \tilde{C} -state of O_3^+ . *Chem. Phys. Lett.*, 375(1):76–83, 2003. ISSN 0009-2614. doi: [https://doi.org/10.1016/S0009-2614\(03\)00818-2](https://doi.org/10.1016/S0009-2614(03)00818-2). URL <https://www.sciencedirect.com/science/article/pii/S0009261403008182>.
- [93] S. M. Younger and T. D. Märk. *Semi-Empirical and Semi-Classical Approximations for Electron Ionization*, chapter 2, pages 24–41. Springer Vienna, Vienna, 1985. ISBN 978-3-7091-4028-4. doi: 10.1007/978-3-7091-4028-4_2. URL https://doi.org/10.1007/978-3-7091-4028-4_2.
- [94] Oleg Zatsarinny and Klaus Bartschat. The B-spline R-matrix method for atomic processes: application to atomic structure, electron collisions and photoionization. *J. Phys. B: At. Mol. Opt. Phys.*, 46(11):112001, May 2013. doi: 10.1088/0953-4075/46/11/112001. URL <https://dx.doi.org/10.1088/0953-4075/46/11/112001>.